

Reassessing quantum-thermodynamic enhancements in continuous thermal machines

José A. Almanza-Marrero¹ and Gonzalo Manzano¹

¹*Institute for Cross-Disciplinary Physics and Complex Systems IFISC (UIB-CSIC),
Campus Universitat Illes Balears, E-07122 Palma de Mallorca, Spain*

(Dated: November 25, 2024)

Quantum coherence has been shown to impact the operational capabilities of quantum systems performing thermodynamic tasks in a significant way, and yet the possibility and conditions for genuine coherence-enhanced thermodynamic operation remain unclear. We show that for steady-state quantum thermal machines —both autonomous and externally driven— that interact weakly with thermal reservoirs and work sources, the presence of coherence induced by perturbations in the machine Hamiltonian guarantees a genuine thermodynamic advantage. Such advantage applies both for the cases in which the induced coherence is between levels with different energies or between degenerate levels. On the other hand, we show that engines subjected to noise-induced coherence, can be outperformed by classical stochastic engines using exactly the same set of (incoherent) resources. We illustrate our results with three prototypical models of heat engines and refrigerators and employ multi-objective optimization techniques to characterize quantum-enhanced regimes in connection with the thermodynamic uncertainty relation and beyond it.

I. INTRODUCTION

The determination of the interplay between quantum coherence —i.e. the ability of quantum systems to exist in superpositions of multiple states— and thermodynamic operation, constitutes one of the main challenges in quantum thermodynamics, attracting increasing attention during the last decade [1, 2]. One of the main approaches to explore this link, in line with the original spirit of thermodynamics, has consisted in the construction and analysis of minimal models of quantum thermal machines showing different types of coherent evolution [3–9]. These machines consist of a quantum system —the working medium— composed by few energy levels or qubits which, by coupling to thermal baths at different temperatures and external work sources, are able to perform useful thermodynamic tasks, such as work extraction, heat pumping, or refrigeration. Recent advances in the manipulation and control of quantum systems in the laboratory allowed the implementation of first prototypes, where the basic principles of these models can be mapped to realistic devices in platforms ranging from ion-traps [10, 11] to NV centers in diamond [12], just to mention a few of them [1, 13].

Since the pioneering works of Scully *et al.* introducing a photo-Carnot engine [14], quantum coherence has been claimed to increase the power output or efficiency of many different types of quantum heat engines and refrigerators. Such improvements are particularly relevant in the case of continuous machines working in steady-state conditions [15], which in principle require less control of the dynamics and couplings with reservoirs. Particularly relevant examples include power-enhancements by noise-induced coherence in lasers, photocell engines, or quantum dots engines [16–18] (with applications in photosynthetic light harvesting [19]), or by input external coherent fields [9, 12], as well as cooling boosts by degenerate coherence in local models of quantum absorption refrigerators [20–22]. In all such cases, coherence has been found

to play a positive role in the output mechanism, eventually leading to an increased ability of the machine for work extraction or refrigeration. However, since all such output mechanisms are model-dependent, it remains unclear whether the performance shown by these machines cannot be achieved by other equivalent classical models [9, 22, 23], so that a truly quantum thermodynamic advantage can be identified. Given the possibility of implementation of these models in the laboratory and their potential applications, clarifying this point becomes an urgent and crucial point to the field.

In this paper we show how to identify genuine coherence-induced quantum thermodynamic advantage and how to quantitatively characterize it in steady-state quantum thermal machines by combining three main ingredients. The first one is the systematic construction of thermodynamically-equivalent classical thermal machines that are able to produce the same average currents than their quantum-coherent counterparts, while using exactly the same amount of incoherent resources (essentially bath temperatures and energy structure). However, even if same average currents can be reproduced by classical models, fluctuations as captured by the variance of the currents might present significant differences. The comparison of fluctuations in the output currents (reliability of the machine) with respect to the classical counterpart is henceforth the second necessary ingredient in our analysis. This is connected with violations in the so-called thermodynamic uncertainty relation (TUR) [24–26], which provides a universal trade-off relation between power, efficiency, and output reliability for any classical Markovian thermal machine operating at steady-state conditions [27]. The TUR sets up a model-independent limit in the maximum reliability achievable by any classical machine at a given power output and efficiency. Hence the observation of TUR violations in quantum Markovian machines working in steady-state conditions [28–33] may be considered as an unambiguous witness of a quantum thermodynamic signature. How-

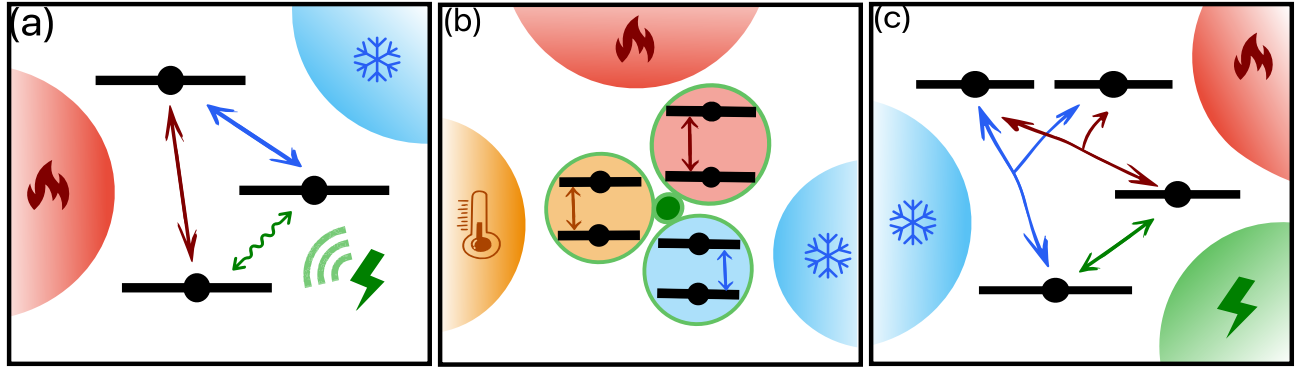


FIG. 1. Schematic representation of three quantum thermal machine models. (a) The coherent three-level amplifier with couplings to baths at hot β_h (red) and cold β_c (blue) temperatures, as well as coherent external driving (green thunderbolt), (b) the three-qubit autonomous (absorption) refrigerator where each qubit is locally coupled to baths at hot (red), cold (blue), and intermediate (yellow) temperatures β_m , and (c) the noise-induced-coherence machine showing collective jumps induced by the baths at hot (red) and cold (blue) temperatures, together with a classical work source given by an infinite-temperature bath (green). Plain double arrows represent jumps between the machine energy levels induced by the baths while wavy arrows represent coherent interactions. Collective jumps in (c) are represented by triple arrows.

ever the contrary is not necessarily true, i.e. the absence of a TUR violation does not imply the absence of thermodynamic enhancements in the machine, as we explicitly show for different classes of quantum machines, like e.g. autonomous multipartite machines. Moreover, the violation of the TUR in specific parameter regimes is not yet a sufficient (nor necessary) condition for ensuring a practical quantum-thermodynamic advantage in thermal machines, since these parameter regimes may be far from optimal performance and therefore be useless after all. The third ingredient that we employ here is then the use of multi-objective optimization techniques (Pareto optimization) [34–39] to actually confirm enhanced stability (precision), power output or efficiency, with respect to classical thermodynamically-equivalent machines, in relevant (optimal) regimes of operation of the machine, such as maximum power conditions.

Our general results show systematic quantum-thermodynamic advantages in the presence of Hamiltonian-induced coherence that are applicable to a broad class of steady-state quantum thermal machines (both autonomous or externally driven) in the weak coupling limit. Moreover, we illustrate our results by employing three well-known (prototypical) models showing coherent-induced evolution (see Fig. 1), each corresponding to one of the three possible types of coherence that can arise in the working medium when approaching the steady state: (a) coherence between different energy levels (energetic coherence) induced by external driving, (b) coherence between levels with degenerate energies induced by internal Hamiltonian couplings, and (c) noise-induced coherence on degenerate levels induced by the reservoir. In the case of Hamiltonian-induced coherence (cases a and b) practical quantum-thermodynamic advantages are unambiguously identified, leading to enhanced optimal regimes not allowed by any equivalent classical engine using the same

amount of thermodynamic resources. On the contrary, noise-induced coherence between degenerate levels (case c) can lead to disadvantages in the performance, even in cases where the quantum machine dynamics contains intrinsic quantum features.

This paper is organized as follows: Sec. II introduces the different thermal machine models in detail. Sec. III discusses how to characterize the thermodynamic performance in such systems. In Sec. IV, we describe the concept of classical equivalent machines and provide a general recipe for constructing them in the presence of different types of coherence. In Sec. V, we show that in the presence of Hamiltonian coherence, quantum improvements over classical equivalent machines can always be achieved for a broad class of quantum models including unicyclic engines and multipartite (multicycle) engines, whereas in the presence of noise-induced coherence, the performance of quantum machines over their classical counterparts depends on the system parameters. In Sec. VI we verify our general statements using three specific models of quantum thermal machines that use different types of coherence to operate. In Sec. VII we optimize both quantum and classical thermal machines and compare their optimal solutions. Finally, Sec. VIII provides a summary and conclusions of our main results.

II. QUANTUM THERMAL MACHINES MODELS

We consider thermal machines running continuously in a steady-state regime described as open quantum systems interacting with two or more thermal baths at different temperatures. The machine system has N energy levels, some of which may be degenerate or not, and interconnected through incoherent transitions mediated by the baths. Moreover, we consider the possibility of one or

more coherent interactions arising as a consequence of one of the three following sources (see Fig. 1): (a) external driving by a classical field (such as in quantum heat engine models of masers and lasers [3–5]); (b) internal Hamiltonian interactions between subsystems in few-body machines (e.g. machines composed by several interacting qubits [6] or harmonic oscillators [7]), and (c) noise-induced coherence caused from collective dissipation acting on two or more resonant transitions (as in some light-harvesting complexes [19] and synthetic heat engine models [17]).

The general Hamiltonian of the machine can be generally written as the sum of two terms:

$$H = H_0 + V(t), \quad (1)$$

where $H_0 = \sum_{i=0}^{N-1} \epsilon_i |i\rangle \langle i|$ is a local Hamiltonian describing N energy levels with $\epsilon_0 \leq \epsilon_1 \leq \dots \leq \epsilon_{N-1}$, and $V(t)$ is a (eventually time-dependent) term capturing coherent transitions between them. It can either represent an external field periodically driving a transition in H_0 , or, in the case of multipartite systems, the internal interaction among machine constituents. An important feature of this interaction Hamiltonian is that it does not severely modify the energy level structure of the system, so that it can be treated as a perturbation to the local Hamiltonian H_0 (i.e. $|V| \ll |H_0|$). On the other hand, for thermal machines using only noise-induced coherence we will typically have $V(t) = 0$ and then $H = H_0$, since that type of coherence appears solely from the effect of the baths. Without loss of generality, we set to zero the ground-state energy of the machine, $\epsilon_0 \equiv 0$.

We are interested in the quantum Markovian dynamics of the machine in the weak coupling regime. Under Born-Markov and secular approximations, it is possible to describe the evolution of the machine state $\rho(t)$ in terms of a quantum master equation in Lindblad form [40–44]:

$$\frac{d\rho(t)}{dt} = \mathcal{L}(\rho) = -i[H(t), \rho(t)] + \sum_{r=1}^R \sum_{k=\uparrow\downarrow} \mathcal{D}_k^{(r)}[\rho(t)], \quad (2)$$

where $H(t)$ is given in Eq. (1) and $\mathcal{D}_k^{(r)}(\rho)$ denote the so-called dissipators, taking into account the effects of dissipative process k from thermal reservoir r on the system (we take $\hbar = 1$ through the paper). These dissipators are given in terms of Lindblad operators $L_k^{(r)}$ associated to each reservoir:

$$\mathcal{D}_k^{(r)}[\rho(t)] := \left(L_k^{(r)} \rho L_k^{(r)\dagger} - \frac{1}{2} \{ L_k^{(r)\dagger} L_k^{(r)}, \rho \} \right). \quad (3)$$

The Lindblad operators $L_k^{(r)}$ here induce jumps between the H_0 levels with fixed energy gap $\Delta\epsilon_k = \pm\Delta\epsilon_r$ determined by bath r , and verify $[H_0, L_k^{(r)}] = -\Delta\epsilon_k L_k^{(r)}$. They can be written in general as:

$$L_k^{(r)} = \sum_{i,j} \alpha_{ij}^k \sqrt{\gamma_{ij}} |j\rangle \langle i|, \quad (4)$$

with $\alpha_{ij}^k = 1$ if $\epsilon_j - \epsilon_i = \Delta\epsilon_k$ and 0 otherwise. In the case of non-degenerate transitions, the above operators reduce to simple jumps $L_k^{(r)} = \sqrt{\gamma_{ij}} |j\rangle \langle i|$ between energy levels $i \rightarrow j$. However, the operators in Eq. (4) can also describe collective jumps where two or more transitions with same (degenerate) gap $\Delta\epsilon_k$ in H_0 may occur simultaneously, e.g. $i \rightarrow j$ and $i \rightarrow j'$ if $\epsilon_j = \epsilon_{j'}$. In any case, every transition is connected to a single thermal bath, the rates $\gamma_{ij} \geq 0$ being time-independent and verifying the local detailed balance relation $\gamma_{ij} = \gamma_{ji} e^{-\beta_r(\epsilon_j - \epsilon_i)}$, with $\beta_r = 1/k_B T_r$ the inverse temperature of the bath r and k_B Boltzmann's constant. In the long-time limit, the evolution dictated by Eq. (3) converges to a steady-state, verifying $\mathcal{L}(\pi) = 0$, where we denote $\pi(t)$ the steady state density operator. We notice that, due to the presence of the time-dependent Hamiltonian $V(t)$, the steady state can show a (residual) periodic time-dependence in the phase in the Schrödinger picture.

Although the results we present apply to any model of quantum thermal machine whose evolution can be described within the general framework introduced above, we will often particularize to three representative and well-known models of quantum thermal machines, as illustrated in Fig. 1. They lead to three different types of coherent evolution respectively: the coherent three-level maser (Fig. 1a) which induces energetic coherence in the H_0 basis; the three-qubit autonomous quantum refrigerator (Fig. 1b), leading to Hamiltonian-induced coherence in a degenerate subspace of H_0 , and the noise-induced-coherence engine (Fig. 1c), showing coherence between degenerate levels induced by collective bath transitions.

A. Coherent three-level amplifier

The three-level maser or amplifier, as initially introduced by Scovil and Schulz-DuBois in Ref. [3], is one of the simplest models of a thermal machine, capable of serving either as a heat engine or a refrigerator depending on the configuration of system parameters [45, 46]. The characteristics and performance of this model has been largely studied [1, 4, 5, 15, 30, 46–49] owing to its simplicity and versatile functionality, and a first experimental implementation has been reported in Ref. [12]. It stands as a main example of a thermal machine where coherence among non-degenerate energy levels is supported in the steady state, suggesting the appearance of regimes where quantum-enhanced thermodynamic operation can be achieved [9] (for a critical view of such quantum-enhanced performance see e.g. Ref. [23]).

The machine system contains three discrete energy levels and an external driving field acting on its lower transition, as depicted in Fig. 1a. The Hamiltonian of the system can be written in this case as:

$$H = \epsilon_1 |1\rangle \langle 1| + \epsilon_2 |2\rangle \langle 2| + V(t), \quad (5)$$

with bare Hamiltonian $H_0 := \epsilon_1 |1\rangle \langle 1| + \epsilon_2 |2\rangle \langle 2|$ time dependent driving Hamiltonian $V(t) = g(e^{-i\omega_d t} |0\rangle \langle 1| +$

h.c) resonant with the first energy gap, i.e. $\omega_d \equiv \epsilon_1$, and where g is the external driving field strength. In the absence thermal baths, this driving field generates Rabi-like oscillations within the first two levels of the machine, $|0\rangle$ and $|1\rangle$, at frequency g .

The two remaining transitions of the three-level system are further weakly coupled to two thermal baths at different inverse temperatures, denoted as cold and hot ($\beta_c \geq \beta_h$), typically modeled as bosonic reservoirs. They lead to four incoherent jumps described by Lindblad operators:

$$\begin{aligned} L_{\downarrow}^{(c)} &= \sqrt{\gamma_{21}} |1\rangle\langle 2|; & L_{\uparrow}^{(c)} &= \sqrt{\gamma_{12}} |2\rangle\langle 1|, \\ L_{\downarrow}^{(h)} &= \sqrt{\gamma_{20}} |0\rangle\langle 2|; & L_{\uparrow}^{(h)} &= \sqrt{\gamma_{02}} |2\rangle\langle 0|, \end{aligned} \quad (6)$$

with rates $\gamma_{21} = \gamma_c(\bar{n}_c + 1)$ and $\gamma_{12} = \gamma_c\bar{n}_c$ associated respectively to the emission and absorption of energy quanta $\Delta\epsilon_c = \epsilon_2 - \epsilon_1$ into the cold reservoir at β_c . Similarly $\gamma_{20} = \gamma_h(\bar{n}_h + 1)$ and $\gamma_{02} = \gamma_h\bar{n}_h$ stand for emission and absorption of energy quanta $\Delta\epsilon_h = \epsilon_2$ into the hot reservoir at temperature β_h . Here γ_r denotes the spontaneous emission rate for bath $r = c, h$ and $\bar{n}_r = (e^{\beta_r\Delta\epsilon_r} - 1)^{-1}$ is the average number of thermal photons with frequency $\Delta\epsilon_r$ in the baths.

As commented before, since we are treating the interaction Hamiltonian as a perturbation, our analysis will be limited to the weak driving regime. In this regime, it is possible to extract the time dependence of the system's Hamiltonian by moving to a rotating frame (interaction picture with respect to H_0). This transformation leads to the following form of the master equation (2):

$$\frac{d\rho'}{dt} = -i[V_I, \rho'] + \sum_{r=c,h} \sum_{k=\downarrow,\uparrow} \mathcal{D}_k^{(r)}[\rho'], \quad (7)$$

where $\rho' = e^{iH_0t}\rho e^{-iH_0t}$ and the driving Hamiltonian in the interaction picture appearing in the Lindblad equation has the simpler form $V_I = g(|0\rangle\langle 1| + |1\rangle\langle 0|)$.

B. Three-qubit autonomous refrigerator

This fridge model was first presented in Ref. [6] and consist of one of the smallest thermal machines models using a multipartite system (see Fig. 1b). It pertains to the class of autonomous quantum refrigerators [8, 50, 51], also called quantum absorption refrigerators [7, 21, 52–55]. It consists of three qubits with different energy gaps, each of them locally coupled to a corresponding thermal baths at a different temperature. A weak three-body energy-preserving Hamiltonian interaction among the qubits allows the generation of heat currents between the three reservoirs that ultimately power thermodynamic tasks such as heat pumping or refrigeration [8]. Different platforms for the actual implementation of this or closely related models in the lab has been proposed using quantum dots [56], optical systems [57], QED arquitectures [58] and trapped ions [11]. In this multipartite setup, genuine quantum features such as quantum

entanglement [20] and discord [52] have been analyzed, suggesting the possibility of boosting the fridge performance by quantum correlations in some operational regimes [20].

The Hamiltonian of the three-qubit working substance here reads:

$$H = H_1 + H_2 + H_3 + V, \quad (8)$$

where we identify $H_0 = \sum_i H_i$ with $H_i = \epsilon_i |1\rangle\langle 1|_i$ the (bare) Hamiltonians of each individual qubit and $V = g(|101\rangle\langle 010| + |010\rangle\langle 101|)$ is a three-body interaction Hamiltonian allowing the qubits to exchange energy (notice the use of the simplified notation $|101\rangle \equiv |1\rangle_1 |0\rangle_2 |1\rangle_3$, etc.). Here above $g \ll \epsilon_i$, ensures that the interaction can be treated as a perturbation to the bare three-qubit Hamitonian H_0 .

Importantly, by assuming the resonance condition $\epsilon_3 = \epsilon_2 - \epsilon_1$, the three qubit interaction verifies strict energy preservation between the qubits, that is $[V, H_1 + H_2 + H_3] = 0$, ensuring that the energy exchanges among the fridge qubits occur without the need of any extra source of energy or control, i.e. preserving the autonomy of the model. At difference from other autonomous fridges, such as single-qutrit fridges [46], this model exhibits steady-state coherence between degenerate energy levels $|101\rangle$ and $|010\rangle$ due to the presence of the interaction V [6], which ultimately leads to entanglement among different partitions involving the qubits [20].

In this case all the transitions are mediated by the reservoirs, with either cold, medium or hot temperatures ($\beta_c \geq \beta_m \geq \beta_h$). Since each qubit i is locally coupled only to a single bath at inverse temperature β_i , and the interaction V is weak, the master equation (2) adopts a local form [42–44], with six incoherent jumps described by Lindblad operators promoting local jumps in each qubit:

$$\begin{aligned} L_{\downarrow}^{(c)} &= \sqrt{\gamma_{10}^c} |0\rangle\langle 1|_1 \otimes \mathbb{1}_2 \otimes \mathbb{1}_3, \\ L_{\downarrow}^{(m)} &= \sqrt{\gamma_{10}^m} \mathbb{1}_1 \otimes |0\rangle\langle 1|_2 \otimes \mathbb{1}_3, \\ L_{\downarrow}^{(h)} &= \sqrt{\gamma_{10}^h} \mathbb{1}_1 \otimes \mathbb{1}_2 \otimes |0\rangle\langle 1|_3, \end{aligned} \quad (9)$$

together with the opposite jumps, $L_{\uparrow}^{(r)} = e^{-\beta_r\Delta\epsilon_r/2} L_{\downarrow}^{(r)\dagger}$, for $r = c, m, h$. The rates $\gamma_{10}^c = \gamma_c(\bar{n}_c + 1)$ and $\gamma_{01}^c = \gamma_c\bar{n}_c$ are associated respectively to the emission and absorption of energy quanta $\Delta\epsilon_c = \epsilon_1$ into the cold reservoir at β_c . Similarly we have $\gamma_{10}^m = \gamma_m(\bar{n}_m + 1)$ and $\gamma_{01}^m = \gamma_m\bar{n}_m$ for the emission and absorption of energy quanta $\Delta\epsilon_m = \epsilon_2$ into the medium reservoir at temperature β_m , as well as $\gamma_{10}^h = \gamma_h(\bar{n}_h + 1)$ and $\gamma_{01}^h = \gamma_h\bar{n}_h$ for the emission and absorption of energy quanta $\Delta\epsilon_h = \epsilon_3$ into the hot reservoir at temperature β_h .

C. Noise-induced-coherence machine

A final set of continuous thermal machines models showing quantum effects, which we collectively dub noise-induced-coherence (NIC) machines, were first presented

in a series of papers by Scully *et al.* [16, 19, 59]. In these machines, degenerate levels in the energy spectrum are combined with a collective action of the baths on the system transitions to generate coherence in the steady state [60, 61]. The operation and performance of these kind of machines has been extensively investigated within the context of quantum thermal machines [17, 18, 22, 48, 62–68], pointing to enhancements in the power output for adequate operational regimes.

A notable example of this coherence is found in a 4-level absorption refrigerator than can also work as a heat engine, whose thermodynamics have been examined in previous studies [66, 68, 69]. In this system, two of the levels possess the same energy, as depicted in Fig. 1c. These levels are subjected to the influence of two distinct thermal baths, whose action results in the emergence of degenerate coherence that persist in the system's steady state. The system's Hamiltonian in this case is as follows

$$H = \epsilon_1 |1\rangle\langle 1| + \epsilon_2 (|2a\rangle\langle 2a| + |2b\rangle\langle 2b|) = H_0. \quad (10)$$

In this case all the transitions are mediated by the reservoirs at cold, hot and “work” temperatures ($\beta_c \geq \beta_h > \beta_w \rightarrow 0$). To represent these transitions we will have six different incoherent jumps, two of them consisting of individual jumps $L_{\downarrow}^{(w)} = \sqrt{\gamma_{10}} |0\rangle\langle 1|$ and $L_{\uparrow}^{(w)} = \sqrt{\gamma_{01}} |1\rangle\langle 0|$, and the other four refer to collective transitions:

$$\begin{aligned} L_{\downarrow}^{(h)} &= \sqrt{\gamma_{a1}} |1\rangle\langle 2a| + \sqrt{\gamma_{b1}} |1\rangle\langle 2b|, \\ L_{\uparrow}^{(h)} &= \sqrt{\gamma_{1a}} |2a\rangle\langle 1| + \sqrt{\gamma_{1b}} |2b\rangle\langle 1|, \\ L_{\downarrow}^{(c)} &= \sqrt{\gamma_{a0}} |0\rangle\langle 2a| + \sqrt{\gamma_{b0}} |0\rangle\langle 2b|, \\ L_{\uparrow}^{(c)} &= \sqrt{\gamma_{0a}} |2a\rangle\langle 0| + \sqrt{\gamma_{0b}} |2b\rangle\langle 0|, \end{aligned} \quad (11)$$

with rates $\gamma_{i1} = \gamma_c^i (\bar{n}_c + 1)$ and $\gamma_{1i} = \gamma_c^i \bar{n}_c$ for $i = a, b$, associated respectively to the emission and absorption of energy quanta $\Delta\epsilon_c = \epsilon_2 - \epsilon_1$ into the cold reservoir at β_c , and similarly $\gamma_{i0} = \gamma_h^i (\bar{n}_h + 1)$ and $\gamma_{0i} = \gamma_h^i \bar{n}_h$ for $i = a, b$, is associated with emission and absorption of energy quanta $\Delta\epsilon_h = \epsilon_2$ into the hot reservoir at temperature β_h . Finally, since the “work” bath is at an infinite temperature i.e $\beta_w \rightarrow 0$ the rates associated to it satisfy $\gamma_{10} = \gamma_{01}$, corresponding in this case for emission and absorption of a quanta $\Delta\epsilon_w = \epsilon_1$ from the work source.

III. THERMODYNAMIC PERFORMANCE

We are interested in the performance of the quantum thermal machine models presented in the previous section when operating in non-equilibrium steady-state conditions [1, 15]. By performance, we refer not only to the size of the output current generated by the machine operation (output power in the case of heat engines or cooling power for the case of refrigerators) and the machine thermodynamic efficiency (ratio of useful output to source input), but also to the size of the fluctuations in

the output current, which can be viewed as measure of the “quality” of that output in stochastic machines [27].

Under steady-state conditions, $\mathcal{L}(\pi) = 0$, the average output power generated by the machine on the external drive and the average heat current absorbed from reservoir r , are given, respectively, by standard definitions [70]:

$$\langle \dot{W} \rangle := -\text{Tr}[\dot{H}(t)\pi(t)] = -\text{Tr}[\dot{V}(t)\pi(t)], \quad (12)$$

$$\langle \dot{Q}_r \rangle := \sum_k \text{Tr}[H_0 \mathcal{D}_k^{(r)}[\pi(t)]], \quad (13)$$

where we recall that $\pi(t)$ may acquire a periodic time-dependence (in Schrödinger picture) due to the presence of non-diagonal elements (coherences) in the steady-state density operator. We also emphasize that for weak perturbations as the ones considered here, only the bare Hamiltonian H_0 enters in the heat currents [71, 72], ensuring consistency with the second law [73] (see also Appendix A). The first law takes the form $\langle \dot{W} \rangle = \sum_r \langle \dot{Q}_r \rangle$, imposing that any output power is sustained by input heat currents from the baths. Explicit expressions of the heat currents $\langle \dot{Q}_r \rangle$ valid for generic machines (with or without degeneracy) are given in Appendix A.

As a consequence of Markovianity, the second law in the setup is manifested through the non-negativity of the entropy production rate:

$$\langle \dot{S}_{\text{tot}} \rangle = -\sum_r \beta_r \langle \dot{Q}_r \rangle \geq 0, \quad (14)$$

which characterizes the irreversibility of the machine operation in its nonequilibrium steady-state [2, 71]. Here it is also work remarking that whenever the temperature of some of the reservoirs r approaches infinity, $\beta_r \rightarrow 0$, the associated energy current does not contribute to the entropy production and hence it should be considered as (incoherent) work rather than heat, see also Refs. [7, 74]. In that case the output power associated to such a work reservoir reads $\langle \dot{W} \rangle = -\sum_k \text{Tr}[H_0 \mathcal{D}_k^{(r)}[\pi(t)]]$.

The efficiency of thermal machines can be defined from the ratio of the average output useful current to the average input resource one, as determined by the operational mode of the machine:

$$\eta := \frac{\langle J_{\text{out}} \rangle}{\langle J_{\text{in}} \rangle}, \quad (15)$$

where in the case of heat engine operation $J_{\text{out}} = \langle \dot{W} \rangle$ and $J_{\text{in}} = \langle \dot{Q}_h \rangle$, while for refrigeration the efficiency (coefficient of performance) is given from $J_{\text{out}} = \langle \dot{Q}_c \rangle$ and either $J_{\text{in}} = -\langle \dot{W} \rangle$ for power-driven refrigerators (as the models in Secs. II A and II C), or $J_{\text{in}} = -\langle \dot{Q}_h \rangle$ for absorption refrigerators (as the one in Sec. II B). For extensions of efficiency to multiple inputs and outputs see e.g. Refs. [75–77].

By combining the first and second laws in the setup we recover Carnot bound for the efficiency of heat engines $\eta \leq \eta_C := 1 - \beta_h/\beta_c$, as well as the corresponding (Carnot) bounds for power-driven fridges $\eta \leq \eta_{\text{fr}} :=$

	Heat engine/pump	Refrigerator
Three-level amplifier	$\omega_d/\epsilon_2 \leq \eta_C$	$\eta_C \leq \omega_d/\epsilon_2 \leq 1$
Autonomous fridge	$\eta_{\text{abs}} \leq \epsilon_1/\epsilon_3 \leq 1$	$\epsilon_1/\epsilon_3 \leq \eta_{\text{abs}}$
NIC machine	$\epsilon_1/\epsilon_2 \leq \eta_C$	$\eta_C \leq \epsilon_1/\epsilon_2 \leq 1$

TABLE I. Parameter relations leading to the main modes of operation of the three thermal machines examined here. In the case of the autonomous (absorption) refrigerator the heat engine regime is replaced by heat pumping.

$\beta_h/(\beta_c - \beta_h)$ and absorption refrigerators, $\eta \leq \eta_{\text{abs}} := (\beta_m - \beta_h)/(\beta_c - \beta_m)$, achieved in the limit of zero entropy production, where all energy currents vanish [1, 15, 50].

The maximum efficiency (zero power) equilibrium points separate the different modes of operation of the machines, where heat currents and output power change sign. In the models presented here they can be easily obtained analytically by noticing that the average steady-state currents can be rewritten as:

$$\langle \dot{Q}_r \rangle = \Delta \epsilon_r \langle \dot{N}_r \rangle, \quad (16)$$

where $\langle \dot{N}_r \rangle$ is the probability current associated to the reservoir r (flux of quanta). It results from the fact that in the models, baths are associated to a single energy gap $\Delta \epsilon_r$. In the steady state, due to the absence of leaks, the system will exchange excitations with all baths at the same rate, i.e. $\forall i, j$ we have $\langle \dot{N}_i \rangle = \langle \dot{N}_j \rangle := \langle \dot{N} \rangle$. In addition, the first law constrains the average value of the work to satisfy $\langle \dot{W} \rangle = \sum_r \Delta \epsilon_r \langle \dot{N} \rangle = \omega_d \langle \dot{N} \rangle$. The ratio between the different steady-state currents hence verify

$$\frac{|\langle \dot{W} \rangle|}{|\langle \dot{Q}_j \rangle|} = \frac{\omega_d}{\epsilon_j} \quad ; \quad \frac{|\langle \dot{Q}_i \rangle|}{|\langle \dot{Q}_j \rangle|} = \frac{\epsilon_i}{\epsilon_j}. \quad (17)$$

By combining the above proportionality relations with the efficiency bounds above, we can construct a table for the operational modes of each model (see Table I).

While it is in general desirable for any thermal machine to have a large output current and a high efficiency (low rate of entropy production), in microscopic systems another fundamental factor to consider is the fluctuations associated with the currents, specially in the output power. Therefore, in addition to minimizing entropy production and maximizing power, low fluctuations (resulting in higher precision) in energy flows are also desirable. In classical systems these three quantities are not independent, but their trade-off is quantified by the TUR:

$$\mathcal{Q} = \langle \dot{S}_{\text{tot}} \rangle \frac{\text{Var}[J_{\text{out}}]}{\langle J_{\text{out}} \rangle^2} \geq 2, \quad (18)$$

where $\langle J_{\text{out}} \rangle$ and $\text{Var}[J_{\text{out}}]$ denote the mean and variance of the useful output current i.e $J_{\text{out}} = \dot{W}, \dot{Q}_c$ for work production and refrigerator regimes respectively. Initially proposed in the context of bio-molecular processes [24], the TUR was then formally established in stochastic thermodynamics [25, 26], and subsequently applied to classical steady-state heat engines [27], for which

the TUR ratio \mathcal{Q} in Eq. (18) can be rewritten in terms of the output power and efficiency as:

$$\mathcal{Q}_{\text{he}} = \beta_c \frac{\text{Var}[\dot{W}]}{\langle \dot{W} \rangle} \left(\frac{\eta_C - \eta}{\eta} \right), \quad (19)$$

where we identified $J_{\text{out}} = \dot{W}$ and $\langle \dot{S}_{\text{tot}} \rangle = -\beta_h \langle \dot{Q}_h \rangle - \beta_c \langle \dot{Q}_c \rangle = \beta_c (\eta_C/\eta - 1) \langle \dot{W} \rangle$. Analogously by taking $J_{\text{out}} = \dot{Q}_c$ and rewriting the expression for the entropy production rate, we obtain the corresponding TUR ratio for power-driven refrigerators:

$$\mathcal{Q}_{\text{fr}} = (\beta_c - \beta_h) \frac{\text{Var}[\dot{Q}_c]}{\langle \dot{Q}_c \rangle} \left(\frac{\eta_{\text{fr}} - \eta}{\eta} \right). \quad (20)$$

Finally, for the case of absorption refrigerators we obtain the TUR ratio:

$$\mathcal{Q}_{\text{abs}} = (\beta_c - \beta_m) \frac{\text{Var}[\dot{Q}_c]}{\langle \dot{Q}_c \rangle} \left(\frac{\eta_{\text{abs}} - \eta}{\eta} \right), \quad (21)$$

where in this case we identified $J_{\text{out}} = \dot{Q}_c$ and the entropy production rate reads $\langle \dot{S}_{\text{tot}} \rangle = -\beta_h \langle \dot{Q}_h \rangle - \beta_c \langle \dot{Q}_c \rangle - \beta_m \langle \dot{Q}_m \rangle = (\beta_c - \beta_m) (\eta_{\text{abs}}/\eta - 1) \langle \dot{Q}_c \rangle$. Throughout this paper, to evaluate fluctuations in the output currents, i.e. the variances $\text{Var}[\dot{W}]$ and $\text{Var}[\dot{Q}_c]$, we employ the full-counting statistics (FCS) formalism [78, 79] (see details in Appendix B).

In any of the three cases, the TUR implies that beyond a certain threshold, a classical Markovian engine can only enhance its precision in the output (cooling) power at the cost of either reducing the output itself or reducing the energy efficiency, so that the above ratio remains bounded by 2, i.e. $\mathcal{Q} \geq 2$. However, some models of quantum thermal machines have been shown to produce violations of the TUR, that is, they verify $\mathcal{Q} < 2$ (see e.g. Refs. [28–33]). Such violations act as a witness indicating an enhanced tradeoff between power, precision and efficiency that arise in certain parameter regimes. Nevertheless, it is in principle unclear whether that violations may occur in relevant regimes, i.e. where the machine performs in an optimal way, providing a practical quantum-thermodynamic advantage. In addition, such quantum-thermodynamic advantages may arise even if the TUR is not violated, since classical machines may not saturate the TUR in such relevant regimes. Hence in order to provide a fair and accurate assessment of quantum-thermodynamic advantages in thermal machines both optimization of the machine performance and comparison to classical models become necessary.

IV. CLASSICAL THERMODYNAMIC EQUIVALENTS OF THERMAL MACHINES

Throughout this paper, inspired by the notion of classical emulability introduced in Ref. [23], we use the term “classical thermodynamic-equivalent” (or simply “classical equivalent”) of a quantum thermal machine to refer

to a thermal machine model with same bare Hamiltonian, H_0 , but whose evolution can be described using only classical Markovian dynamics (stochastic jumps between the energy levels), while being capable of producing the same average currents as the quantum machine, by using the same amount of incoherent resources. Notice that if the classical equivalent machine is capable of producing the same average currents, this ensures the same power output and efficiency as the original quantum machine. However, quantum and classical equivalent models may differ in general in their fluctuations.

By using same incoherent resources we mean that the classical-thermodynamic equivalent model is in contact with the same thermal baths, and therefore have access to the same temperatures. Furthermore, the requisite of having same bare Hamiltonian H_0 implies that the classical equivalent also has the same energy level structure as the original quantum machine, which allow us to identify them as the “same machine”. This is in contrast with other notions of classical analogs in thermal machines where all the parameters of the classical model are imposed to be exactly equal, including the couplings to the baths or the driving strength [9, 12] (this is also the case of introducing extra dephasing in the quantum model). Here instead we allow to vary these parameters as long as the requirements for weak-coupling and Markovian dynamics assumed for the thermal machine models are satisfied. This choice is not arbitrary, but allows for an stronger notion of genuine quantum-thermodynamic advantage that avoids spurious “advantages” that may disappear by just slightly modifying some of the parameters in the classical model.

In the following, we develop a general method for constructing these equivalent machines in situations where the coherence in the system arises either from Hamiltonian dynamics (Hamiltonian-induced coherence) or from dissipative processes (noise-induced coherence).

A. Hamiltonian-induced coherence

Since we want the classical equivalent to produce the same average energy currents than the quantum counterpart, our starting point will be the generic expression for the heat currents given in Eq. (13). This expression, valid for any given (bare) Hamiltonian H_0 , can be rewritten as (see App. A):

$$\langle \dot{Q}_r \rangle = \sum_{i < j}^{\in B_r} (\epsilon_j - \epsilon_i) (\gamma_{ij} \pi_{ii} - \gamma_{ji} \pi_{jj}), \quad (22)$$

where we remind the reader that transitions in the sum above are restricted to the ones induced in the set B_r , i.e. induced by reservoir r . The above expression only depends on the level populations (diagonal elements of the density matrix), energy gaps of the machine and jump rates. As a consequence, the useful output current of the machine can only depend on these quantities as follows

from the first law, e.g. in heat engines $\langle \dot{W} \rangle = \sum_r \langle \dot{Q}_r \rangle$. Given that the energy gaps and temperatures of the reservoirs are fixed, we conclude that to ensure identical input and output currents, the quantum machine and its classical equivalent must have matching diagonal elements in their steady-state density matrices.

In order to mimic the same level populations in the classical equivalent, we proceed by first solving the equations of motion for the diagonal elements and non-vanishing coherences in the quantum machine (details of this procedure are presented in Appendix C). Let’s denote by indices $|u\rangle$ and $|v\rangle$ a couple of levels that are connected by V (for simplicity we assume $|u\rangle$ and $|v\rangle$ not further connected to other levels). The equations of motion for these two levels read:

$$\begin{aligned} \dot{\rho}_{uu} &= \sum_{j \neq u} \gamma_{ju} \rho_{jj} - \rho_{uu} \sum_i \gamma_{ui} - 2g \text{Im}(\rho_{uv}), \\ \dot{\rho}_{vv} &= \sum_{j \neq v} \gamma_{jv} \rho_{jj} - \rho_{vv} \sum_i \gamma_{vi} + 2g \text{Im}(\rho_{uv}), \\ \dot{\rho}_{uv} &= -\frac{1}{2} \sum_i (\gamma_{ui} + \gamma_{vi}) \rho_{uv} - ig (\rho_{vv} - \rho_{uu}), \end{aligned} \quad (23)$$

while for the rest of levels $n \neq \{u, v\}$, not connected by V , we simply have $\dot{\rho}_{nn} = \sum_{j \neq n} \gamma_{jn} \rho_{jj} - \rho_{nn} \sum_i \gamma_{ni}$.

Following Ref. [23], by equating all the derivatives to zero in Eqs. (23), we can determine the relation between the coherence of levels connected by the Hamiltonian V and their populations (that should be verified in the steady state):

$$\pi_{uv} = \frac{-2ig(\pi_{vv} - \pi_{uu})}{\sum_i (\gamma_{ui} + \gamma_{vi})}. \quad (24)$$

Then we introduce the above dependence back into off-diagonal elements in Eqs. (23), to obtain that the net effect of coherence in the steady state is equivalent to adding a virtual transition promoting jumps between the interacting levels $|u\rangle$ and $|v\rangle$:

$$\begin{aligned} \frac{d}{dt} \rho_{uu} &= \sum_{j \neq u} \gamma_{ju} \rho_{jj} - \rho_{uu} \sum_i \gamma_{ui} + \gamma_{vu}^{\text{cl}} \rho_{vv} - \gamma_{uv}^{\text{cl}} \rho_{uu}, \\ \frac{d}{dt} \rho_{vv} &= \sum_{j \neq v} \gamma_{jv} \rho_{jj} - \rho_{vv} \sum_i \gamma_{vi} + \gamma_{uv}^{\text{cl}} \rho_{uu} - \gamma_{vu}^{\text{cl}} \rho_{vv}, \end{aligned} \quad (25)$$

with transition rates

$$\gamma_{uv}^{\text{cl}} = \gamma_{vu}^{\text{cl}} = \frac{4g^2}{\sum_i (\gamma_{ui} + \gamma_{vi})}. \quad (26)$$

As a consequence, if we replace the Hamiltonian term V responsible for the coherent interaction between levels $|u\rangle$ and $|v\rangle$ by the above extra stochastic transition between them, the system governed by Eqs. (25) will reach an steady-state with exactly the same populations as the original one governed by Eq. (23), and therefore the same currents in Eq. (22).

We have thus achieved a classical equivalent of the quantum model in which the dynamics is entirely classical, as given by a set of incoherent jumps between the machine energy levels, while reproducing the same (average) currents in the steady state. We also notice that the equivalent machine is coupled to the same set of thermal baths, while the coherent interaction is replaced by an stochastic jump process without bias in either direction. This provides a classical equivalent model that uses the same amount of incoherent resources. In the case of energetic coherence, i.e. non-degenerate levels $|u\rangle$ and $|v\rangle$ ($\epsilon_u \neq \epsilon_v$) this means replacing the quantum-coherent work source (battery) by a classical stochastic work source (battery), like a bath at infinite temperature. On the other hand, in the case of degenerate coherence ($\epsilon_u = \epsilon_v$) the extra stochastic transition is a source of pure noise without any associated energy current and can hence be considered as free.

B. Noise-induced coherence

In this case, we find that the heat currents of the collective transitions explicitly depend on the real part of the coherence between energy levels involved in the environmental noise-inducing mechanism (which we again denote $|u\rangle$ and $|v\rangle$):

$$\begin{aligned} \langle \dot{Q}_r \rangle = & \sum_{i < j} (\epsilon_j - \epsilon_i) (\gamma_{ij} \pi_{ii} - \gamma_{ji} \pi_{jj}) \\ & + 2 \sum_j (\epsilon_j - \epsilon_v) (\gamma_{uj} + \gamma_{vj}) \text{Re}(\pi_{uv}), \end{aligned} \quad (27)$$

while the currents that are not involved in the noise-inducing mechanism are given by Eq. (22) as in the previous case (see App. A). Moreover, in Appendix C we show that reproducing the steady-state populations results again in equal average currents, despite of the appearance of the second contribution in Eq. (27).

Following the same procedure as for Hamiltonian-induced coherence, we can observe the net effect of coherence in the steady state by solving the equations of motion and replacing the dependence of coherence back into the equations (see details in App. C):

$$\pi_{uv} = \frac{\sum_i [2\sqrt{\gamma_{ui}\gamma_{vi}}\pi_{ii} - \sqrt{\gamma_{iu}\gamma_{iv}}(\pi_{uu} + \pi_{vv})]}{\sum_i (\gamma_{iu} + \gamma_{iv})}. \quad (28)$$

As before, we obtain a virtual jump between the coherent levels u and v , but in this case we also find corrections to the rates in some of the (already present) jumps involving these levels and other levels of the machine n . Thus the rates for the classical equivalent must be of the form:

$$\begin{aligned} \gamma_{uv}^{\text{cl}} = \gamma_{vu}^{\text{cl}} &= \frac{\left(\sum_j \sqrt{\gamma_{uj}\gamma_{vj}} \right)^2}{\sum_j (\gamma_{uj} + \gamma_{vj})}, \\ \gamma_{in}^{\text{cl}} &= \gamma_{in} - 2\sqrt{\gamma_{un}\gamma_{vn}} \gamma_{uv}^*, \\ \gamma_{ni}^{\text{cl}} &= \gamma_{ni} - 2\sqrt{\gamma_{nu}\gamma_{nv}} \gamma_{uv}^*, \end{aligned} \quad (29)$$

where $i = u, v$ above and we defined $\gamma_{uv}^* := \sum_j \sqrt{\gamma_{uj}\gamma_{vj}} / \sum_j (\gamma_{uj} + \gamma_{vj})$. It can be proved that local detailed balance relations are not modified in any transition of the machine by the corrections to the rates above. To show this, let us rewrite the rates of the collective transitions to and from levels $i = \{u, v\}$ as $\gamma_{in} = \gamma_r^i \exp[\beta_r(\epsilon_i - \epsilon_n)/2]$ and $\gamma_{ni} = \gamma_r^i \exp[-\beta_r(\epsilon_i - \epsilon_n)/2]$ respectively, were $\gamma_r^i := \sqrt{\gamma_{in}\gamma_{ni}}$ is a purely kinetic (spontaneous-emission-like) contribution to the rates not depending on the direction of the jumps, and β_r is the temperature of the bath to which the transition is coupled. Using this notation the corrected rates read

$$\begin{aligned} \gamma_{in}^{\text{cl}} &= (\gamma_r^i - 2\gamma_{uv}^* \sqrt{\gamma_r^u \gamma_r^v}) \exp[\beta_r(\epsilon_i - \epsilon_n)/2], \\ \gamma_{ni}^{\text{cl}} &= (\gamma_r^i - 2\gamma_{uv}^* \sqrt{\gamma_r^u \gamma_r^v}) \exp[-\beta_r(\epsilon_i - \epsilon_n)/2]. \end{aligned} \quad (30)$$

Notice that the corrections only affect the purely kinetic contributions to the rates, but not their bias. As a consequence, the classical equivalent will employ the same thermodynamic resources (temperatures and energy gaps) as the quantum system. In other words, in order to construct the classical equivalent machine we can replace the collective transitions appearing in the original quantum model by local ones (with a tuned rate) to the same thermal baths, and add an extra stochastic transition between the degenerated levels $|u\rangle$ and $|v\rangle$.

V. THERMODYNAMIC IMPACT OF COHERENCE

We are now in a position to present our general results that unveil the impact of steady-state coherence in the performance of quantum thermal machines by direct comparison with the classical thermodynamic-equivalent machine introduced above. We recall that, by construction, the classical equivalent machine reproduces the same average currents in all the transitions, and hence it has the same efficiency than the original machine. However, fluctuations in the output current (as captured by the variance), can differ in general between quantum and classical models, making the presence of coherence either beneficial or detrimental for the machine output reliability. In the following, we show that Hamiltonian coherence always lead to reliability improvements (for same output and efficiency), while thermal machines operating with noise-induced coherence can either perform better or worse than their classical-equivalent counterparts.

In order to address the impact of coherence in the reliability of the thermal machines, we introduce the relative difference in the fluctuations between classical and quantum machines as

$$\mathcal{R} := \frac{\text{Var}[J_{\text{out}}^{\text{cl}}] - \text{Var}[J_{\text{out}}]}{\text{Var}[J_{\text{out}}]}, \quad (31)$$

where $J_{\text{out}}^{\text{cl}}$ denotes the output current in the classical thermodynamic-equivalent model. The above ratio measures the relative reduction in the dispersion of the output current in the quantum machine, as compared to the

classical one. If $\mathcal{R} < 0$, then the classical equivalent provides a more accurate output than the original quantum one; $\mathcal{R} = 0$ implies that the quantum and classical models are indistinguishable from their dispersion, and $\mathcal{R} > 0$ implies that the output in the quantum machine is more accurate, hence providing a quantum-thermodynamic advantage manifested in an enhanced reliability of the machine for same average output and efficiency.

Our aim here is to obtain analytical expressions for the variances of the output currents for generic quantum machines and its classical equivalent counterpart by using the full counting statistics formalism, in order to construct the relative difference \mathcal{R} in Eq. (31) and evaluating its sign. This can be performed in principle for both cases of Hamiltonian-induced coherence and noise-induced coherence, following respectively Secs. IV A and IV B. We will first focus on the case of Hamiltonian-induced coherence, since it is in that case that more universal results can be obtained, and then discuss also the case of noise-induced coherence.

As we have seen in Sec. IV a set of rate equations for the evolution of the populations and coherence is be obtained for both the original quantum engine and its classical equivalent counterpart, which for Hamiltonian-induce coherence are given in Sec. IV A. However, we notice that even assuming a single transition with coherence, the general N -level problem is composed by $N - 2$ equations of the form:

$$\dot{\rho}_{nn} = \sum_{j \neq n} (\gamma_{jn}\rho_{jj} - \gamma_{ni}\rho_{nn}) \quad (32)$$

plus 3 more equations for the coherent subspace in the quantum machine, Eqs. (23), or 2 for equations for the classical equivalent, Eqs. (25); with the additional simplification that in steady state conditions, we have $\dot{\rho}_{nn} = 0 \forall n$. As a consequence, it is clear that in order to obtain analytical results in the generic case, we need to reduce the dimension of the problem. Here, we are able to reduce (and fix) the dimension of the machine by introducing a “coarse grained” mesostate, similar to the one presented in Ref. [80], involving almost all of the incoherent transitions as follows.

More precisely, we define a “mesostate” $|S\rangle$ that comprises $N - 3$ levels of the thermal machine that are not involved in the coherent interaction (see Fig. 2 for a diagram). We keep outside $|S\rangle$ only the coherent subspace (levels $|u\rangle$ and $|v\rangle$) and an extra level (denoted without loss of generality as $|m\rangle$ for “monitoring”) connected to it by at least one stochastic transition mediated by a thermal bath (here $|v\rangle \leftrightarrow |m\rangle$ without loss of generality), that allow us to properly apply the full counting statistics formalism to uncover the fluctuations in the flux over that transition [81].

Being composed by an ensemble of levels, the occupation probability of the mesostate can be written as

$$\rho_{SS} := \sum_{j \in S} \rho_{jj}, \quad (33)$$

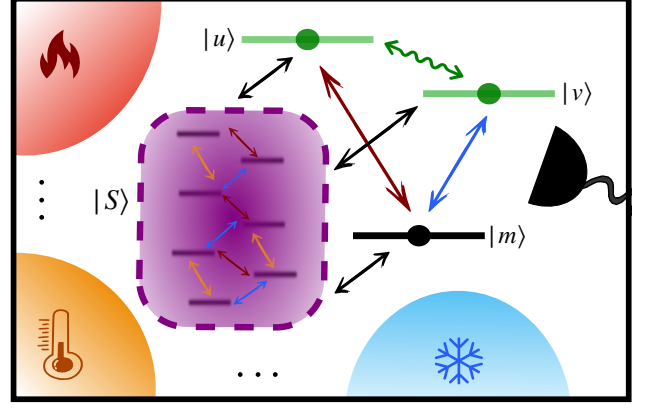


FIG. 2. Schematic representation of a generic N level thermal machine with Hamiltonian-induced coherence in a subspace composed by two levels (green levels). The transitions between all other levels are produced by thermal baths at possibly different temperatures (simple arrows), and one of its transitions is being monitored (black detector). A reduced version of the machine model is obtained by introducing the coarse-grained state S (purple shaded box) including $N - 3$ levels. In the unicycle case the rates of the transitions $|v\rangle \leftrightarrow |S\rangle$ and $|u\rangle \leftrightarrow |m\rangle$ are set to zero, as well as the transitions between levels within the coarse-grained state $|S\rangle$ leading to multiple cycles.

verifying that $\sum_{i \notin S} \rho_{ii} + \rho_{SS} = 1$. Moreover effective rates for the transitions involving the mesostate and any other level i can be defined as

$$\Gamma_{Si} := \frac{1}{\rho_S} \sum_{j \in S} \gamma_{ji} \rho_{jj}, \quad ; \quad \Gamma_{iS} := \sum_{j \in S} \gamma_{ij}, \quad (34)$$

where only the rates of transitions going “out” of the mesostate Γ_{Si} to the other levels depend on the steady state populations. Then by introducing the mesostate S , the $N - 2$ set of equations (32) can be reduced to the following 2 equations

$$\begin{aligned} \dot{\rho}_{mm} &= \sum_{i \notin S} (\gamma_{im} \rho_{ii} - \gamma_{mi} \rho_{mm}) + \Gamma_{Sm} \rho_{SS} - \Gamma_{mS} \rho_{mm}, \\ \dot{\rho}_{SS} &= \sum_{i \notin S} (\Gamma_{iS} \rho_{ii} - \Gamma_{Si} \rho_{SS}). \end{aligned} \quad (35)$$

to be combined with Eqs. (23) for the coherent levels in the quantum machine model, or with Eqs. (25) for the corresponding classical equivalent machine. In any case these extra equations remain unchanged by the substitution of the remaining levels by the mesostate $|S\rangle$.

Notably, with the above procedure we have fixed the dimension of the general problem to a 4-states thermal machine with coherence between two of these states. That means applying FCS with a matrix of dimension 5 in the quantum case and of dimension 4 for the classical thermodynamic-equivalent machine (see Appendix B). Here it is also important to notice that, by allowing transitions between $|S\rangle$ and all the other (three) states of the

machine (as well as transitions among the levels within S), this general procedure applies to thermal machines that can be both unicycle or multicyclic, where the unicycle case is recovered by setting to zero the rates of the transition $|v\rangle \leftrightarrow |S\rangle$ and $|u\rangle \leftrightarrow |m\rangle$.

The next step is to obtain analytical expressions for the variance of the current in the monitored transition $|v\rangle \leftrightarrow |m\rangle$. This is done for both the quantum machine and its classical counterpart. Here it is important to mention that, in order to assess the fluctuations of the relevant steady-state currents (including coherent work in the transition $|u\rangle \leftrightarrow |v\rangle$) from FCS in a single transition of the machine, we have to impose some specific conditions on the transition structure of the machine. In particular, we assume that every transition in the machine is coupled to a single thermal reservoir and that quanta are conserved in all interactions with the reservoirs in the weak-coupling limit, which can be considered as mild conditions. A more restrictive condition is that all thermal reservoirs must contribute the same number of quanta in all the cycles present in the original machine (including those closed by the coherent transitions). This condition (trivially) includes unicycle machines, but also a broad class of multicycle structures that we dub "symmetric multicycle" machines. A relevant example of those structures are obtained in multipartite scenarios like the three-qubit fridge introduced in Sec. II B, for which all possible cycles involve the exchange of one quantum with each reservoir. This is also the case for many other engines and refrigerators, such as e.g. continuous versions of the SWAP engine [82], fridges made up of bosonic modes [7, 11] or using optomechanical-like couplings [83], as well as quantum dot devices [56, 84], just to mention a few.

In all these situations, the variances of the currents are proportional to each other, $\text{Var}[\dot{Q}_r] = \Delta\epsilon_r^2 \text{Var}[\dot{N}]$ for all reservoirs r with $\text{Var}[\dot{N}] := \text{Var}[\dot{N}_l] \forall l$, and also $\text{Var}[\dot{W}] = \omega_d^2 \text{Var}[\dot{N}]$ for the power output (see also App. B). Therefore, the relative difference in the fluctuations in Eq. (31) can be conveniently rewritten as:

$$\mathcal{R} := \frac{\text{Var}[\dot{N}^{\text{cl}}] - \text{Var}[\dot{N}]}{\text{Var}[\dot{N}]}, \quad (36)$$

where $\text{Var}[\dot{N}^{\text{cl}}]$ denotes the corresponding variance of the current in the classical equivalent model. The explicit expressions for $\text{Var}[\dot{N}]$, $\text{Var}[\dot{N}^{\text{cl}}]$ are provided in Appendix D for a generic quantum machine with N levels and 1 coherent transition. In the case of more than 1 (independent) coherent transitions, they can be handled by using the same techniques independently for every coherent subspace, all of which are kept outside the coarse-grained state S (hence augmenting the effective dimension of the system as a counterpart).

Once the general expressions for the variances are obtained, the sign of \mathcal{R} can be evaluated to observe its universal character. We resume the result of this analysis enunciating the following theorem, whose explicit demon-

stration can be found in Appendix E:

Theorem 1 *Under the presence of Hamiltonian-induced coherence, quantum thermal machines in the weak coupling limit outperform the precision of their classical thermodynamic-equivalent counterparts (as defined as in Sec. IV) in steady-state conditions. In particular it is verified that the relative difference in the fluctuations is always strictly positive $\mathcal{R} > 0$ when the systems are in out-of-equilibrium conditions and becomes zero in equilibrium.*

The above theorem means that out of equilibrium, the quantum thermal machine is always more precise than its classical thermodynamic equivalent. Since the classical thermodynamic equivalent will have by construction equal average output currents and efficiency than the quantum machine, that implies that Hamiltonian-induced coherence invariably leads to quantum-thermodynamic advantages. In other words, there is no classical model that using the same resources can reproduce the power, efficiency and reliability of the quantum thermal machine.

Theorem 1 is a main result of our fluctuation analysis that applies to generic unicyclic and symmetric multicycle quantum thermal machines operating in nonequilibrium stationary states (NESS) in the weak coupling regime and under weak driving or perturbations, so that their evolution is describable by the Lindblad master equation, Eq. (2). Examples of such thermal machines are ubiquitous [1], comprising few level masers and lasers under weak driving [12, 47, 85, 86], superconducting devices [33, 87, 88], or many-body engines [32, 89], as well as a number of autonomous engines, refrigerators and quantum clock models [56–58, 90–92] composed by various units that interact weakly among them.

The impact of coherence in the case of noise-induced coherence can be also analyzed using a similar method than in the Hamiltonian case. However in this case more complications arise. The set of rate equations describing the evolution of the system are given in Appendix C [Eqs. (C6) and (C7)]. In that case, a mesostate similar to the one above might be introduced, but it can only include all the machine levels that are not directly connected to the coherent subspace spanned by states u and v . All other state transitions will be now affected by the presence of the coherent transition [c.f. Eq. (29)] and the allowed parameter regimes need to ensure their positivity. Moreover, the intrinsic multicyclic structure no longer ensures that the variances of the steady-state currents in all the transitions are equal as before, but the results may depend on the chosen level to perform the FCS monitoring.

As a consequence, contrary to the Hamiltonian-induced case, the impact of noise-induced coherence turns out to be not universal and depends on the specific model, the specific parameters of the machine, and the specific transition in which FCS is performed, leading to the following:

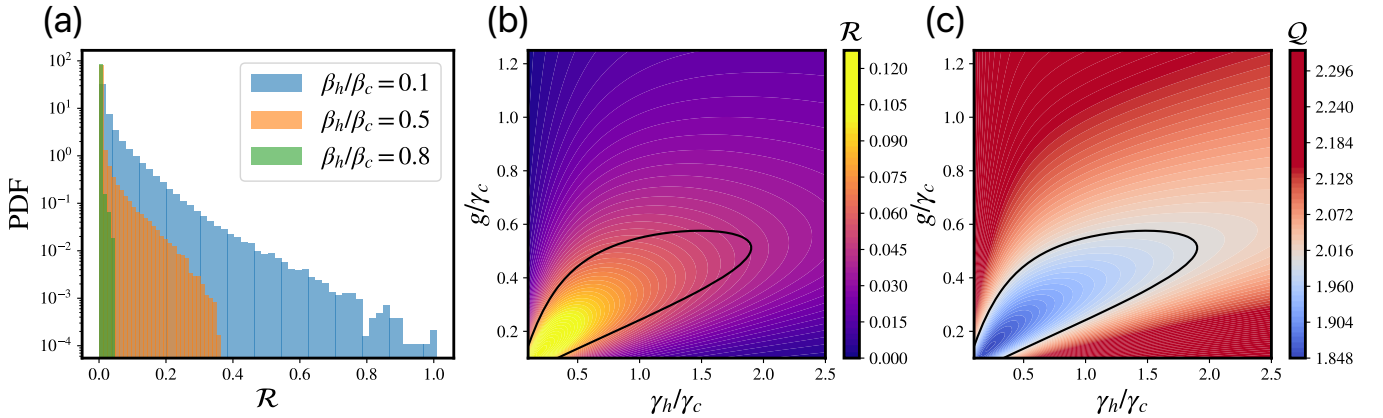


FIG. 3. a) Histogram of sampled values of the ratio between the fluctuations of the system and its classical analog \mathcal{R} for different ratios of the bath temperatures (see legend). The values corresponds to an exploration of the following region in the parameters space of the system: $\beta_c = 1$, $\epsilon_2 = 5$, $\omega_d \in [0.1, 4.9]$, $\gamma_{h/c} \in [10^{-5}, 10^{-2}]$ and $g \in [10^{-5}, 10^{-2}]$. b) Colour maps of the fluctuation ratio \mathcal{R} and c) the TUR ratio Q_{he} as a function of the bath interaction strengths and the driving force. The other systems parameters are: $\beta_c = 1$, $\beta_h = 0.1/\beta_c$, $\epsilon_2 = 5$, $\omega_d = 2.5$ and $\gamma_c = 10^{-3}$ (energies are given in $k_B T_c = 1$ units).

Theorem 2 *Under the presence of noise-induced coherence, quantum thermal machines in the weak coupling limit can either outperform or be outperformed by their classical thermodynamic-equivalent counterparts (as defined as in Sec. IV) in steady-state conditions. In particular the relative difference in the fluctuations \mathcal{R} can be either positive or negative depending on the specific parameters of the machine.*

The proof of this theorem is provided in the next section and follows from constructing and analyzing a (counter)example, the NIC machine introduced in Sec. II C where regimes with either $\mathcal{R} > 0$ and $\mathcal{R} < 0$ are founded for different parameter regimes. The importance of Theorem 2 relies in that it puts firmer criteria for the classification of quantum-thermodynamic advantages in noise-induced machines that the ones previously considered in the literature, such as the consideration of the dephased model [16–19], and going beyond the absence of TUR violations, as it has been checked in some noise-induced models, see e.g. Ref. [68].

In the following section we illustrate our results for the three prototypical machines introduced before, showing the advantages produced by Hamiltonian-induced coherence in the first two models (both for energetic and degenerate coheres) and determining the range of parameters in which the third one (the NIC engine) leads to advantages and disadvantages with respect to its classical equivalent counterpart, suggesting the careful revision of previous claims for quantum-advantages in this type of machines.

VI. ILLUSTRATIVE EXAMPLES

We now illustrate our results for the three paradigmatic examples of quantum machines discussed in Sec. II

constructing explicitly their classical equivalent machines and assessing the role of the coherence in the fluctuations of the currents. We numerically generate a 10^6 number of possible system configurations in the whole parameter space, that verify the basic assumptions that ensure the consistency of the Markovian dynamics, and perform a direct comparative analysis between quantum and classical models.

A. Three level amplifier

Following the general recipe provided in Sec. IV, the classical equivalent of the three-level amplifier can be obtained by replacing the driving Hamiltonian $V(t)$ by an extra stochastic transition between levels $|0\rangle$ and $|1\rangle$. The rates of these extra transitions, as given by Eq. (26) become $\gamma_{01}^{\text{cl}} = \gamma_{10}^{\text{cl}} = 4g^2/(\gamma_h \bar{n}_h + \gamma_c \bar{n}_c)$.

In order to quantify the impact of (energetic) coherence in the three-level amplifier, we compute the fluctuations ratio \mathcal{R} in Eq. (31) for the output power, $J = \dot{W}$. Exploring the model parameters for fixed external temperatures of the baths, we observe the appearance of a significant amount of configurations with $\mathcal{R} > 0$, that increases as the temperature bias powering the machine increases. This is illustrated in Fig. 3a where the distribution of \mathcal{R} values over 10^6 configurations is shown for three different choices of (fixed) environmental temperatures. As can be appreciated, for all configurations we obtain $\mathcal{R} \geq 0$, that is, the three-level amplifier always match or exceed the performance of the corresponding classical equivalent machine for each configuration, hence unveiling a beneficial role of energetic coherence. Improvements reaching an output power variance reduction up to $\mathcal{R} \sim 1$ are possible for temperature bias of the order $T_h = 10T_c$. We also observe a fat tail in the distribution that ensures the robustness of the enhancements, meaning that

many configurations can lead to significant reductions in the output variance. The range of variance reductions shrinks towards higher \mathcal{R} values as the temperature bias is reduced, and tends to disappear close to equilibrium (similar temperatures of the baths) where quantum and classical models perform almost equally. This effect is a manifestation of the nonequilibrium character of the enhancements produced by energetic coherence.

In Fig. 3b the behaviour of the fluctuations reduction ratio, \mathcal{R} in Eq. (31), is plotted as a function of the spontaneous emission rates and the driving strength. Darker colours denote regions where larger stability enhancements with respect to the classical equivalent machine are obtained, which are verified in the regime of very weak driving and highly asymmetric spontaneous rates (low coupling strength with the hot bath as compared to the cold one). This plot can be contrasted with Fig. 3c where the TUR ratio in Eq. (19) is shown for the same range of parameters. In both plots the black solid line has been introduced as a guide to the eye representing the boundary ($\mathcal{Q}_{\text{he}} = 2$) of the region where TUR violations are obtained. This allows the comparison of the method using the classical equivalent machine to detect quantum-thermodynamic enhancements, with the direct search for violations of the (classical) TUR [28–33].

We observe that the area where violations of the TUR, $\mathcal{Q}_{\text{he}} < 2$, are verified, is contained within the region $\mathcal{R} > 0$ and indeed coincide with the highest improvements in precision as measured by the reduction ratio \mathcal{R} . However, as expected, we also find that even in regimes where the TUR is not violated, there exists an improvement in accuracy of the output current due to the presence of energetic coherence. Therefore, using the classical equivalent of the original three level amplifier, we are able to identify regimes of thermodynamic enhancement that cannot be revealed by violations of the TUR.

B. Three-qubit autonomous refrigerator

For the autonomous refrigerator model, we find that the classical equivalent is obtained by replacing the three-body interaction Hamiltonian V allowing the exchange of energy between qubits, by a classical transition producing incoherent jumps between levels $|101\rangle$ and $|010\rangle$. The rate of this transition, according to Eq. (26) becomes in this case $\gamma_{uv}^{\text{cl}} = \gamma_{vu}^{\text{cl}} = 4g^2 / \sum_r (2\bar{n}_r + 1)\gamma_r$, where $|u\rangle = |101\rangle$ and $|v\rangle = |010\rangle$, and the sum runs over the three baths, $r = \text{h, m, c}$.

For assessing the enhancements in the reliability of the refrigerator, the relative fluctuations \mathcal{R} in Eq. (31) is computed for the cooling power (heat current from the cold bath), $J_{\text{out}} = \dot{Q}_c$. The distributions for the reduction ratio \mathcal{R} and TUR ratio \mathcal{Q}_{abs} (inset) in this case are shown in Fig. 4 again for 10^6 parameter configurations. As can be observed, in this case we obtain $\mathcal{R} \geq 0$ for all configurations, meaning that a reduction of the fluctuations ratio is always possible. As a consequence, we

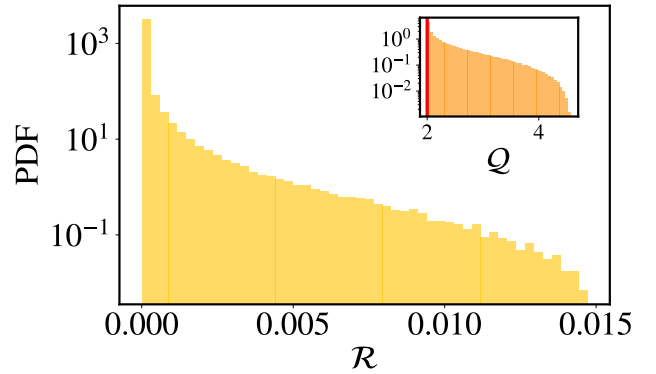


FIG. 4. Histogram of sampled values of \mathcal{Q} (inset plots) and the ratio between the fluctuations of the system and its classical equivalent R (outset plots). The values corresponds to an exploration of the following region in the parameters space of the system: $\beta_c = 1$, $\beta_m/\beta_c \in [0, 1]$, $\beta_h/\beta_m \in [0, 1]$, $\epsilon_2 = 5$, $\epsilon_1 \in [0.1, 4.9]$, $\gamma_{c/m/h} \in [10^{-5}, 10^{-2}]$ and $g \in [10^{-4}, 10^{-2}]$ (energies are given in $k_B T_c = 1$ units).

have to conclude that the three-qubit quantum refrigerator performs better than its classical equivalent, despite it has been shown to operate using entanglement [20]. In particular, in the majority of cases, the fluctuations in both systems are comparable, with certain cases where the quantum system exhibits noise levels up to 1.5% lower than its classical thermodynamic equivalent. Looking at the distribution of \mathcal{Q}_{abs} values, we also see that the autonomous refrigerator remains unable to break the classical constraint imposed by the TUR in all system configurations (inset plot).

C. Noise-induced coherent machine

In the case of the NIC machine, previous studies have shown that when the rates of the collective transitions were equal ($\gamma_{na} = \gamma_{nb}$ and $\gamma_{an} = \gamma_{bn}$ for $n = 0, 1$) it is possible to apply a change of variables that effectively decouples coherences from populations [66] (see also Ref. [71] for a similar case). However, such change of variables does not produce this decoupling when the rates are unequal, suggesting that the system enters a purely quantum regime [69]. In the following, we show that in both cases a classical equivalent can be defined for large regions of the parameter space, that can be used to evaluate the thermodynamic impact of noise-induced coherence.

We first introduce the following basis change within the coherent subspace, where the degenerate levels $|2a\rangle$ and $|2b\rangle$ are transformed into levels $|\alpha\rangle$ and $|\beta\rangle$, with:

$$|\alpha\rangle = \frac{1}{\sqrt{\gamma_c^a + \gamma_c^b}} \left(\sqrt{\gamma_c^a} |2a\rangle + \sqrt{\gamma_c^b} |2b\rangle \right), \quad (37)$$

$$|\beta\rangle = \frac{1}{\sqrt{\gamma_c^a + \gamma_c^b}} \left(\sqrt{\gamma_c^b} |2a\rangle - \sqrt{\gamma_c^a} |2b\rangle \right).$$

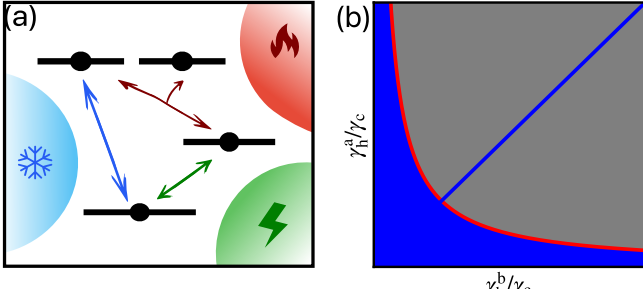


FIG. 5. (a) Schematic representation of the level transitions in the NIC machine after the change of variables. Here one of the double coherent transitions are replaced by a simple jump ($|0\rangle \leftrightarrow |\alpha\rangle$). (b) Graphical representation of the inequality (40) for $\gamma_h^a = \gamma_h^b =: \gamma_c$, separating the regimes where we can define the classical equivalent for noise-induced coherence (blue zone) and where we cannot (grey zone). In the symmetric case (blue diagonal) the classical equivalent can always be defined.

Notice that in the case of symmetric rates for the cold reservoir, $\gamma_c^a = \gamma_c^b$, this expression becomes the one presented in Ref. [69], but differs otherwise. By introducing this change, we successfully decouple the state $|\beta\rangle$ from the state $|0\rangle$, resulting in a machine with only one explicit collective transition, as illustrated in Fig. 5 (see Appendix for more detailed information).

Following Sec. IV B, the classical equivalent of the NIC machine includes an extra stochastic transition between the degenerate levels reading:

$$\gamma_{\alpha\beta}^{\text{cl}} = \gamma_{\beta\alpha}^{\text{cl}} = \frac{(\bar{n}_h + 1)^2 \gamma_h^\alpha \gamma_h^\beta}{(\bar{n}_c + 1) \gamma_c^\alpha + (\bar{n}_h + 1)(\gamma_h^\alpha + \gamma_h^\beta)}, \quad (38)$$

together with corrections to the rates of the collective transitions

$$\begin{aligned} \gamma_{k1}^{\text{cl}} &= \left(\gamma_h^k - \frac{2\gamma_{\alpha\beta}^{\text{cl}}}{\bar{n}_h + 1} \right) (\bar{n}_h + 1), \\ \gamma_{1k}^{\text{cl}} &= \left(\gamma_h^k - \frac{2\gamma_{\alpha\beta}^{\text{cl}}}{\bar{n}_h + 1} \right) \bar{n}_h, \end{aligned} \quad (39)$$

for $k = \alpha, \beta$. By examining the above equations, we find that the corrections to the spontaneous emission rates can make these rates eventually negative, which would correspond to a nonphysical situation. Consequently, the construction of the classical equivalent for noise-induced coherence is limited to scenarios that ensure positive rates in Eq. (39). For the NIC machine analyzed here, this happens when

$$\begin{aligned} \gamma_h^\beta &= 0; \quad \gamma_h^\alpha > 0, \\ \gamma_h^\beta &> 0; \quad \gamma_h^\alpha > \gamma_h^\beta; \quad \frac{(\gamma_h^\alpha - \gamma_h^\beta)}{\gamma_c^\alpha} \leq \frac{\bar{n}_c + 1}{\bar{n}_h + 1}, \\ \gamma_h^\beta &> 0; \quad \gamma_h^\alpha \leq \gamma_h^\beta; \quad \frac{(\gamma_h^\beta - \gamma_h^\alpha)}{\gamma_c^\alpha} \leq \frac{\bar{n}_c + 1}{\bar{n}_h + 1}, \end{aligned} \quad (40)$$

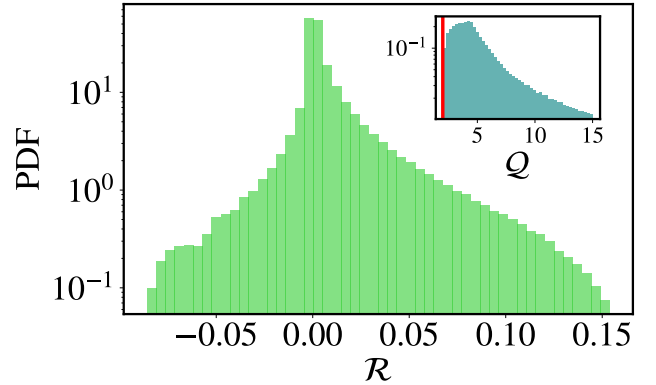


FIG. 6. Histogram of sampled values of \mathcal{Q} (inset plots) and the ratio between the fluctuations of the system and its classical equivalent \mathcal{R} (outset plots). The values corresponds to an exploration of the following region in the parameters space of the system: $\beta_w \rightarrow 0$, $\beta_c = 1$, $\beta_h/\beta_c \in [0, 1]$, $\epsilon_2 = 5$, $\epsilon_1 \in [0.1, 4.9]$, $\gamma_h^{(a/b)} \in [10^{-5}, 10^{-2}]$ and $\gamma_c^{(a/b)} = 10^{-3}$ (energies are given in $k_B T_c = 1$ units).

which, taking into account the variable change together with $\bar{n}_h \geq \bar{n}_c$, corresponds to the stimulated emission rate in the cold bath being greater than or equal to the difference in stimulated emission rates in the hot bath between transitions from levels $|\alpha\rangle$ and $|\beta\rangle$.

We obtain analytically the fluctuation ratio \mathcal{R} in Eq. (31) for the NIC machine and its classical equivalent, taking again $J_{\text{out}} = \dot{W}$. By evaluating the expression for 10^6 different parameter configurations within the region where the classical equivalent machine can be defined, we show in Fig. 6 the distribution of \mathcal{R} together with the corresponding distribution of the TUR ratio Q_{he} values (see inset). Our results show that $\mathcal{R} \geq 0$ for some configurations, pointing to quantum-thermodynamic advantages in a similar way than the two previous examples. However, here we also get configurations leading to $\mathcal{R} < 0$. For that configurations the quantum-coherent machine becomes more noisy than its classical equivalent, hence leading to a detrimental role for the coherence. Indeed for some configurations the NIC machine reaches noise levels up to 1% higher than its classical counterpart. Moreover, by looking at the inset we observe that, as expected, the TUR is not violated for all choices of parameters ($Q_{\text{he}} \geq 2$ always) in accordance to previous studies about TUR violations in similar models [68].

Therefore, it becomes clear that the NIC machine is able to overcome the classical equivalent machine in some configurations which are not witnessed by TUR violations as in the case of Hamiltonian-induced coherence between degenerate levels; but not in all configurations. Contrary to the case of Hamiltonian-induced coherence, noise-induced one has not necessarily a beneficial impact in the thermodynamic performance of the NIC machine, whose operation in terms of power, efficiency and reliability can be surpassed in some regimes by a purely classical

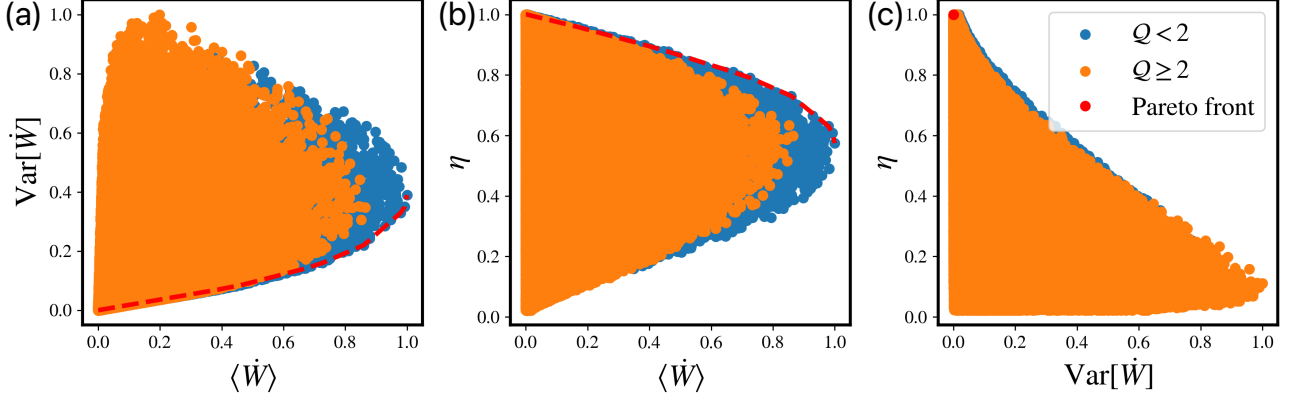


FIG. 7. Violations of the TUR and two dimensional multi-objective optimization for power $\langle \dot{W} \rangle$, power fluctuations $\text{Var}[\dot{W}]$ and efficiency η for the Coherent three-level amplifier. Points are generated from 10^5 different configurations in the parameter space $\omega_d \in [0.1, 4.9]$, $\gamma_{h/c} \in [10^{-5}, 10^{-2}]$ and $g \in [10^{-5}, 10^{-3}]$ and fixed $\beta_c = 1$, $\beta_h = 0.1$, $\epsilon_2 = 5$ (energies are given in $k_B T_c = 1$ units). Blue points represent configurations that violate the classical TUR and Pareto fronts to the red dashed line (see legend). Axes are normalized by the respective maximum values $\langle \dot{W} \rangle_{\text{max}} = 9.5 \times 10^{-4} k_B T_c / \hbar$, $\text{Var}[\dot{W}]_{\text{max}} = 5.1 \times 10^{-3} (k_B T_c / \hbar)^2$, and $\eta_C = 0.9$.

equivalent machine using the same set of resources.

The region of parameters in which a quantum-thermodynamic advantage over the classical equivalent is verified can be obtained analytically (see App. C) and is given by:

$$\frac{\gamma_h^\alpha}{\gamma_h^\beta} \geq \frac{2 + 3(\bar{n}_h + \bar{n}_c) + 4\bar{n}_h\bar{n}_c}{\bar{n}_h - \bar{n}_c}, \quad \gamma_h^\beta \neq 0. \quad (41)$$

Detrimental effects from coherence are obtained for regions where the above inequality is inverted. In particular, in the symmetric case $\gamma_c^a = \gamma_c^b$ and $\gamma_h^a = \gamma_h^b$ we will have that $\gamma_h^\beta = 0$ and the system effectively becomes a three level system without coherence in the steady state. In this limit, the quantum system and its classical analog become indistinguishable. These conclusions are in contrast with some previous claims in the literature claiming quantum enhancements (also in the symmetric case) for same or similar NIC models, see e.g. Refs. [16–19], which lacked a careful comparison to classical thermodynamic-equivalent models.

VII. PARETO OPTIMIZATION AND PRACTICAL ADVANTAGES

In the previous sections we have seen that only for the case of Hamiltonian-induced coherence, corresponding e.g. to the cases of the three-level amplifier introduced in Sec. II A and to the three-qubit refrigerator in Sec. II B, a quantum-thermodynamic advantage is guaranteed in out-of-equilibrium conditions for all range of parameters. In that case, there is a net reduction of the output current fluctuations as compared to classical equivalent machines operating at same (average) output power and efficiency, hence providing performances not achievable with classical stochastic machines using the

same amount of resources. Still in order to proof a practical (and hence useful) advantage, an analysis of the regimes where such an improved reliability is obtained is needed. Here we show that the advantages identified before occur indeed along optimal performance, e.g. for maximum power and for maximum efficiency regimes.

Since optimizing the machine performance involves more than one desired objective (maximize power, maximize efficiency, minimize fluctuations), multi-objective optimization techniques, also called Pareto optimization, are required. These techniques are well known in engineering [93] and have been applied to a wide range of problems, from network theory [34] to betting strategies [35] and phenotypic response [36]. They have also attracted some attention recently in the field of stochastic and quantum thermodynamics, where they have been applied to the optimization of heat engine cycles in the slow-driving regime [37–39].

In order to solve a multi-objective optimization problem (let's take for example a two-dimensional problem) we first define a utility function that depends on the quantities to be optimized (e.g. maximization of power and minimization of fluctuations) with the form

$$\Omega := \lambda \langle \dot{W} \rangle - (1 - \lambda) \text{Var}[\dot{W}], \quad (42)$$

where the parameter λ takes values in the range $[0, 1]$. The role of the parameter λ is to give weights to the two objectives, thus defining a single optimization problem for the whole function Ω . By maximizing Ω we obtain solutions that are both optimal in terms of maximizing power and minimizing fluctuations according to a fixed weight λ . For $\lambda = 0$ we recover the problem of only minimizing fluctuations (whose solution is the zero fluctuations point), while in the case $\lambda = 1$ we recover the problem of only maximizing power (leading to the maximum power point). Indeed varying λ we obtain a family

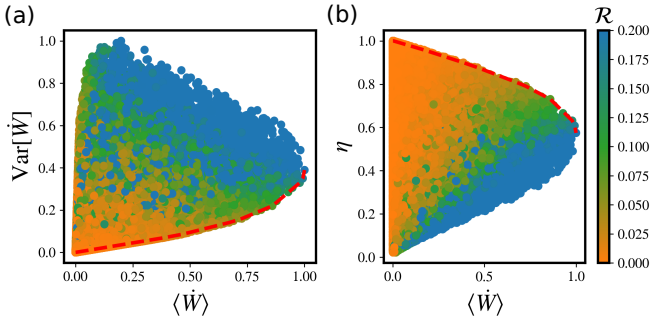


FIG. 8. Fluctuations ratio and two dimensional multi-objective optimization of power $\langle \dot{W} \rangle$, power fluctuations $\text{Var}[\dot{W}]$ and efficiency η for the Coherent three-level amplifier. Points are generated from 10^5 different configurations in the parameter space $\omega_d \in [0.1, 4.9]$, $\gamma_{h/c} \in [10^{-5}, 10^{-2}]$ and $g \in [10^{-5}, 10^{-3}]$ and fixed $\beta_c = 1$, $\beta_h = 0.1$, $\epsilon_2 = 5$ (energies are given in $k_B T_c = 1$ units). The color scale stands for the fluctuation ratio \mathcal{R} and Pareto fronts are highlighted in red (see legend). Axes are normalized by the respective maximum values $\langle \dot{W} \rangle_{\max} = 9.5 \times 10^{-4} k_B T_c / \hbar$, $\text{Var}[\dot{W}]_{\max} = 5.1 \times 10^{-3} (k_B T_c / \hbar)^2$, and $\eta_C = 0.9$.

of standard optimization problems for a single variable, Ω . The solution to the multi-objective optimization problem —the so-called Pareto front— is hence constructed by combining the solutions for every single-objective optimization problems, i.e. for all $\lambda \in [0, 1]$.

We applied the above optimization technique to the prototypical models introduced in Sec. II for numerically obtaining Pareto fronts to three different multi-objective optimization problems, each of which optimizing two of the three performance indicators of the machine, namely average output power $\langle \dot{W} \rangle$, efficiency η and power fluctuations $\text{Var}[\dot{W}]$. For illustrative purposes we focus first on the three-level amplifier of Sec. II A, and then on the three-qubit autonomous refrigerator of Sec. II B.

In Fig. 7 we can see the shape of the Pareto front (red curves) of the three-level amplifier for the three different optimization problems with fixed environmental temperatures and varying ω_d , γ_h , γ_c and g . There, each circle (independently of its color) is generated from a possible configuration (choice of parameters) of the machine. For the optimization problems involving maximizing power $\langle \dot{W} \rangle$ and minimizing fluctuations $\text{Var}[\dot{W}]$ (Fig. 7a) or maximizing power $\langle \dot{W} \rangle$ and minimizing efficiency η (Fig. 7b), the Pareto fronts include a whole branch of solutions indicating a trade-off between the optimization objectives. These go from the zero fluctuations point to the maximum power one in the first case, and from the Carnot point to maximum power point in the second one. On the other hand, for the problem of minimizing fluctuations $\text{Var}[\dot{W}]$ and maximizing efficiency η (Fig. 7c) the Pareto front collapses to a single point, or optimal solution, achieving zero fluctuations and Carnot efficiency (but at zero output power).

The role of coherence in the performance of the en-

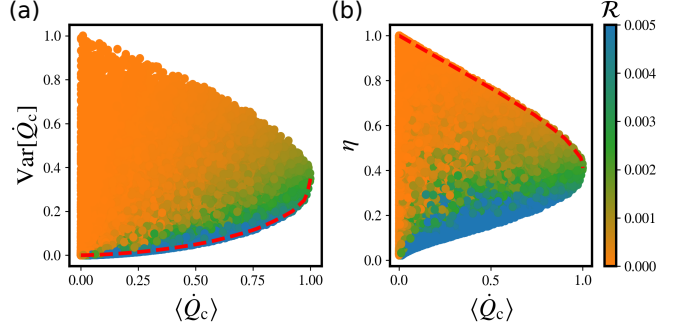


FIG. 9. Fluctuations ratio and two dimensional multi-objective optimization of cooling power $\langle \dot{Q}_c \rangle$, its fluctuations $\text{Var}[\dot{Q}_c]$ and the coefficient of performance η for the three-qubit autonomous refrigerator. Points are generated from 10^5 different configurations in the parameter space $\epsilon_1 \in [0.1, 4.9]$, $\gamma_{h/m/c} \in [10^{-5}, 10^{-2}]$ and $g \in [10^{-5}, 10^{-3}]$ and fixed parameters $\beta_c = 1$, $\beta_m/\beta_c = 0.5$, $\beta_h/\beta_c = 0.05$, $\epsilon_2 = 5$ (energies are given in $k_B T_c = 1$ units). Axes are normalized by the respective maximum values $\langle \dot{Q}_c \rangle_{\max} = 2.9 \times 10^{-4} k_B T_c / \hbar$, $\text{Var}[\dot{Q}_c]_{\max} = 2.4 \times 10^{-3} (k_B T_c / \hbar)^2$, and $\eta_{\text{abs}} = 0.9$.

gine can be unveiled by coloring the circles representing each parameter configuration according to their value of the TUR ratio \mathcal{Q}_{he} (orange for $\mathcal{Q}_{\text{he}} \geq 2$ and blue for TUR violations, $\mathcal{Q}_{\text{he}} < 2$). As can be appreciated in Fig. 7, in all cases the configurations that violate the TUR span the domain classically achievable. More importantly, in Figs. 7a and 7b, we observe TUR violations within the Pareto fronts for large power outputs, and including the maximum power point. This result implies that the coherent three-level amplifier shows a quantum-thermodynamic advantage (as spotted by the violation of the TUR) in relevant regimes of operation, where the machine performs in an optimal way. The TUR violations in Fig. 7 are to be compared with the value of the fluctuations ratio \mathcal{R} for the same parameter configurations in the optimization problems, as shown in Fig. 8 for power and fluctuations (a), and power and efficiency (b). As predicted by Theorem 1 in Sec. V, we obtain positive values $\mathcal{R} > 0$ except at zero power, when equilibrium is reached. Moreover, the presence of large values of \mathcal{R} along the Pareto front confirm the presence of practical quantum-thermodynamic advantages in optimal regimes of operation for $\langle \dot{W} \rangle > 0$, where the largest values of \mathcal{R} are obtained at the maximum power point.

On the other hand, for the three-qubit autonomous refrigerator, the TUR is never violated and hence it cannot be used to spot practical advantages in optimal operation regimes. In this case, our method is nevertheless able to show that practical quantum-thermodynamic advantages can be obtained despite the absence of TUR violations, as predicted by Theorem 1 in Sec. V. In Fig. 9 we show the colormap of \mathcal{R} for the corresponding two optimization problems of the three-qubit refrigerator with fixed environmental temperatures and varying ω_d , γ_h , γ_c and g . The corresponding Pareto fronts are shown again in red

color, which have qualitatively similar shapes as in the coherent three-level amplifier [Fig. 8]. Also for this case, Fig. 9 reveals that configurations with values of $\mathcal{R} > 0$ are obtained along the Pareto fronts, confirming the presence of quantum-thermodynamic advantages produced by the presence of degenerate coherence in optimal regimes of operation. In this case, maximum values appear along all the Pareto front $\text{Var}[\dot{Q}_c] - \langle Q_c \rangle$. However, we observe that the values of \mathcal{R} are in general much smaller than in the previous case, showing a higher impact of energetic coherence to produce quantum advantages in comparison to degenerate one.

VIII. CONCLUSIONS

We have characterized the thermodynamic impact of Hamiltonian and noise-induced coherence in the performance of quantum thermal machines operating in nonequilibrium steady states. While machines displaying Hamiltonian coherence in their steady states lead to quantum-thermodynamic advantages in terms of their tradeoff between power, efficiency and stability, this is not always the case for machines displaying noise-induced coherence. These results, obtained through direct comparison of generic quantum thermal machines with axiomatically-constructed classical equivalent models, ensure the presence of quantum-enhanced performance for models of Hamiltonian-induced coherence in out of equilibrium situations. On the other hand, they also imply that several previous claims of thermodynamic advantages in machines with noise-induced coherence may be spurious, and suggests that they should be reassessed on a case-by-case basis, by determining the set of parameters in which quantum advantages may really exist (if any). Indeed, even if the dynamics of these machines may exhibit purely quantum features, a classical Markovian machine using the same set of resources (energy gaps and bath temperatures) can be systematically constructed that performs just as well or better than the original machine.

The classical equivalent model employed here allowed us a comparison of the current fluctuations between a quantum device and a classical (incoherent) counterpart that outputs the same average currents while employing identical thermodynamic resources. This notion of classical equivalent machine constructs on the idea of emulability discussed in Ref. [23], and is accompanied by a general methodology for its derivation in generic cases. The classical equivalent can be constructed for virtually any quantum steady-state machine working in the weak-coupling regime, and under weak-driving conditions, namely, when the driving can be considered a perturbation of the (bare) machine Hamiltonian. Extensions of this method to the case of strong couplings or strong periodic driving (e.g. using Floquet formalism) are an interesting direction for future research which may allow addressing quantum-thermodynamic advantages in

a larger class of quantum devices.

Using the three-level amplifier and the three-qubit-fridge as main examples of a quantum thermal machines displaying Hamiltonian coherence (the first energetic coherence and the second degenerate one), we have illustrated situations where coherence is always beneficial. In these cases the performance match or exceeds the performance of its classical equivalent counterpart in all possible configurations, with improvements in the machine stability that become greater far from equilibrium. In the case of the three-level amplifier, the parameter regions where these improvements are maximal coincide indeed with regimes where the thermal machine breaks the TUR bound. However, we also observe wide regions showing (smaller) thermodynamic improvements that are not witnessed by TUR violations. This is indeed entirely the case for the three-qubit-fridge, where the TUR by itself is not able to spot thermodynamic enhancements. Importantly, our results reveal that in order to observe a genuine quantum-thermodynamic advantage, it is necessary (and sufficient) to consider the fluctuations in the currents (at least at the level of the variance), in contrast to previous assessments based on more limited notions of classical equivalents (leading also to a less stringent comparison) [9].

Beyond the direct comparison between quantum machines and their respective equivalents for given parameters, we also provided an all-to-all comparison computing the optimal configurations (Pareto front) of quantum and classical machines maximizing power and efficiency while minimizing fluctuations. Our analysis reveals that quantum-thermodynamic advantages in both the three-level amplifier and the three-qubit-fridge occur indeed within the optimal front, allowing thus for a practical quantum-thermodynamic advantage. However, it is also clear from our analysis that in the three-qubit-fridge, the advantages are much lower than in the three-level amplifier. Since implementations of these or similar thermal machine models have been proposed in a number of platforms [13, 56–58, 87], and have been actually experimentally realized with NV-centers in diamond [12] and trapped ions [11] respectively, it would be interesting to test our results for the quantum-thermodynamic advantages reported here in relevant regimes by suitably measuring the variance of the currents [94, 95].

ACKNOWLEDGMENTS

We thank Roberta Zambrini for comments and interesting discussions. We wish to acknowledge support from the María de Maeztu project CEX2021-001164-M for Units of Excellence and CoQuSy project PID2022-140506NB-C21, funded by MICIU/AEI/10.13039/501100011033/FEDER, UE. GM acknowledges the Ramón y Cajal program RYC2021-031121-I funded by MICIU/AEI/10.13039/501100011033 and European Union NextGenerationEU/PRTR. JAAM

acknowledges the Conselleria d'Educació, Universitat i Recerca of the Balearic Islands (Grant FPI-FPI.058.2022).

Appendix A: General expression of current first moments with local dissipation

In this appendix we derive a general expression for the average heat currents including the cases in which coherence may be generated either by Hamiltonian or noise-induced sources. We start by expanding the expression for the standard definition for the heat currents as given in Eq. (13), that is:

$$\begin{aligned} \langle \dot{Q}_r \rangle &= \sum_k \text{Tr}[(H_0 + V(t))\mathcal{D}_k^{(r)}[\pi(t)]] \\ &= \sum_k \text{Tr}[H_0 \mathcal{D}_k^{(r)}[\pi(t)]] = \sum_k \text{Tr}[\mathcal{D}_k^{\dagger(r)}[H_0]\pi(t)] \\ &= \sum_k \sum_{m,l} \langle m | L_k^{(r)\dagger} H_0 L_k^{(r)} - \frac{1}{2} \{ L_k^{(r)\dagger} L_k^{(r)}, H_0 \} | l \rangle \pi_{lm} \end{aligned} \quad (\text{A1})$$

where the terms $\text{Tr}[V(t)\mathcal{D}_k^{(r)}[\pi(t)]] \sim g\gamma_0^k$ have been neglected in accordance to the weak coupling and weak driving approximations. We have applied the cyclic property of the trace to obtain the adjoint dissipator $\mathcal{D}_k^{\dagger(r)}[\cdot] := L_k^{(r)\dagger} \cdot L_k^{(r)} - \frac{1}{2} \{ L_k^{(r)\dagger} L_k^{(r)}, \cdot \}$. Now, using the explicit form of the Lindblad operators in Eq. (4) and the bare Hamiltonian, $H_0 = \sum_i \epsilon_i |i\rangle \langle i|$, we can obtain each term in the sum of the last expression:

$$\begin{aligned} L_k^{(r)\dagger} H_0 L_k^{(r)} &= \sum_{i,j,n} \sqrt{\gamma_{ij}\gamma_{nj}} \epsilon_j |i\rangle \langle n| \delta(\Delta\epsilon_{ji} - \Delta\epsilon_k) \delta(\Delta\epsilon_{ni}), \\ L_k^{(r)\dagger} L_k^{(r)} H_0 &= \sum_{i,j,n} \sqrt{\gamma_{ij}\gamma_{nj}} \epsilon_n |i\rangle \langle n| \delta(\Delta\epsilon_{ji} - \Delta\epsilon_k) \delta(\Delta\epsilon_{ni}), \\ H_0 L_k^{(r)\dagger} L_k^{(r)} &= \sum_{i,j,n} \sqrt{\gamma_{ij}\gamma_{nj}} \epsilon_n |n\rangle \langle i| \delta(\Delta\epsilon_{ji} - \Delta\epsilon_k) \delta(\Delta\epsilon_{ni}), \end{aligned} \quad (\text{A2})$$

where the δ functions arise from the fact that the Lindblad operators produce jumps only between levels with a fixed energy gap $\Delta\epsilon_k = \pm\Delta\epsilon_r$, determined by the reservoirs and we used $\delta(\Delta\epsilon_{ji} - \Delta\epsilon_k)\delta(\Delta\epsilon_{jn} - \Delta\epsilon_k) = \delta(\Delta\epsilon_{ji} - \Delta\epsilon_k)\delta(\Delta\epsilon_{ji} - \Delta\epsilon_{ij}) = \delta(\Delta\epsilon_{ji} - \Delta\epsilon_k)\delta(\Delta\epsilon_{ni})$. By introducing the expressions in (A2) into (A1) we arrive at a general expression for the heat currents valid for both degenerate and non-degenerate level structures in the machine:

$$\begin{aligned} \langle \dot{Q}_r \rangle &= \sum_{k,n,i,j} \sqrt{\gamma_{ij}\gamma_{nj}} \delta(\Delta\epsilon_{ji} - \Delta\epsilon_k) \delta(\Delta\epsilon_{ni}) \\ &\quad \times [\epsilon_j \pi_{ni} - \epsilon_n \text{Re}(\pi_{ni})]. \end{aligned} \quad (\text{A3})$$

If we now particularize the above expression for the case where we don't have degenerate energy levels, the

term $\delta(\epsilon_{ni})$ leads to select indices with $n = i$ and we arrive to:

$$\begin{aligned} \langle \dot{Q}_r \rangle &= \sum_{k,i,j} \delta(\Delta\epsilon_{ji} - \Delta\epsilon_k)(\epsilon_j - \epsilon_i) \gamma_{ij} \pi_{ii} \\ &= \sum_{i < j} (\epsilon_j - \epsilon_i) (\gamma_{ij} \pi_{ii} - \gamma_{ji} \pi_{jj}), \end{aligned} \quad (\text{A4})$$

as given in Eq. (22). On the other hand, for the cases with degenerate energy levels, $\delta(\epsilon_{ni})$ can be zero even for $n \neq i$, and extra terms are obtained. In the case of a single pair of degenerate levels $|u\rangle$ and $|v\rangle$ we obtain:

$$\begin{aligned} \langle \dot{Q}_r \rangle &= \sum_{i < j} (\epsilon_j - \epsilon_i) (\gamma_{ij} \pi_{ii} - \gamma_{ji} \pi_{jj}) \\ &\quad + 2 \sum_j (\epsilon_j - \epsilon_v) (\gamma_{uj} + \gamma_{vj}) \text{Re}(\pi_{uv}) \end{aligned} \quad (\text{A5})$$

as we reported in Eq. (27). Notice above that the extra term in the heat current, which is associated to transitions to or from the degenerate levels, is indeed non-zero only in the presence of coherence between the degenerate pair $\pi_{uv} \neq 0$. Moreover, the coherence needs to have a real component, as it is the case of the noise-induced-coherence machine, c.f. (28). On the other hand, in the case of autonomous refrigerators showing Hamiltonian-induced coherence, the coherence between degenerate levels in the steady state is a pure imaginary number [c.f. Eq. (24)], and the heat current hence reduces to the standard expression for non-degenerate levels, as in Eq. (A4).

Appendix B: Full Counting Statistics

The Full Counting Statistics (FCS) formalism is used to compute the variances of the different input and output currents of the quantum thermal machines presented and their classical equivalent models. In this formalism a set of counting fields $\vec{\chi} := \{\chi_r\}$ are introduced that keep track of the exchanges of energy quanta between the machine and the thermal reservoirs r . These lead to the derivation of a generalized master equation for an extended density operator $\rho_G(t, \{\chi_r\})$ depending on the fields. It reads [78]:

$$\begin{aligned} \frac{d}{dt} \rho_G(t, \{\chi_r\}) &= -i [H(t), \rho_G(t, \{\chi_r\})] \\ &\quad + \sum_{r=1}^R \sum_k \bar{\mathcal{D}}_k^{(r)} [\rho_G(t, \{\chi_r\})], \end{aligned} \quad (\text{B1})$$

with a new set of dissipators with a modified form:

$$\begin{aligned} \bar{\mathcal{D}}_k^{(r)} [\rho_G] &:= e^{-\nu_k^{(r)} \chi_r} L_k^{(r)} \rho_G L_k^{(r)\dagger} \\ &\quad - \frac{1}{2} \left\{ L_k^{(r)\dagger} L_k^{(r)}, \rho_G \right\}. \end{aligned} \quad (\text{B2})$$

where the numbers $\nu_k^{(r)}$ are chosen to be 1 for operators $L_k^{(r)}$ associated with the emission of a quanta into the reservoir r ($\Delta\epsilon_k = -\Delta\epsilon_r$) and -1 for operators associated with the absorption of a quanta ($\Delta\epsilon_k = \Delta\epsilon_r$). In this way, the counting fields χ_r are associated to the net flux of quanta \dot{N}_r transferred from the reservoir into the machine.

In any case, in the limit $\{\chi_r\} \rightarrow 0$, we recover $\rho_G(t) = \rho(t)$ and (B1) reduces to the standard master equation (2) for the machine evolution. Moreover, as in the case of the original master equation, Eq. (B1) can be linearized and written in the form

$$d\vec{p}_G(t)/dt = W_G(\{\chi_r\})\vec{p}_G(t), \quad (\text{B3})$$

where $\vec{p}_G(t)$ contains all the density operator elements and W_G is a matrix capturing the dependence between elements ρ_{ij} within the set of equations of motion. We are interested in the eigenvalue $\lambda(\{\chi_r\})$ of the matrix W_G with the largest real part, which is related to the machine cumulant generating function $\mathcal{K}(\chi_r, t)$. Indeed for systems with a single steady state we have that in the long time limit [96]:

$$\mathcal{K}(\{\chi_r\}, t) \rightarrow \lambda(\{\chi_r\})t. \quad (\text{B4})$$

Then the cumulants $\mathcal{C}_n^{(r)}$ associated to the exchange of quanta with the different reservoirs corresponding to the counting fields χ_r , can be obtained as derivatives with respect to that counting fields of this eigenvalue, evaluated for all fields equal to zero:

$$\mathcal{C}_n^{(r)} = (-i\partial_{\chi_r})^n \lambda(\{\chi_i\})|_{\{\chi_i\}=0}, \quad (\text{B5})$$

for $n = 1, 2, 3, \dots$. Here the first ($n = 1$) and second ($n = 2$) cumulants correspond, respectively, to the average ($\mathcal{C}_1^{(r)} = \langle \dot{N}_r \rangle$) and variance ($\mathcal{C}_2^{(r)} = \text{Var}[\dot{N}_r]$) of the currents of quanta on that reservoir. The average and variances of the heat currents in which we are mainly interested in this work are then given by:

$$\langle \dot{Q}_r \rangle = \Delta\epsilon_r \mathcal{C}_1^{(r)}, \quad \text{Var}[\dot{Q}_r] = \Delta\epsilon_r^2 \mathcal{C}_2^{(r)}. \quad (\text{B6})$$

Due to the preservation of quanta exchanges in all the interactions in the weak coupling limit, it follows that for long trajectories in steady-state machines where the different reservoirs contribute the same number of quanta along all possible cycles, we have a proportionality among all currents. That means that the fluctuations of every current are also proportional:

$$\begin{aligned} \text{Var}[\dot{Q}_r] &= \Delta\epsilon_r^2 \text{Var}[\dot{N}], \\ \text{Cov}[\dot{Q}_r \dot{Q}_s] &= \Delta\epsilon_r \Delta\epsilon_s \text{Var}[\dot{N}], \end{aligned} \quad (\text{B7})$$

where $\text{Var}[\dot{N}] = \text{Var}[\dot{N}_r]$ for all r . Analogously, the average and variance of the power for the case of external driving are given, respectively, by the first law,

$\langle \dot{W} \rangle = \sum_r \langle \dot{Q}_r \rangle$, and in the long-time limit we have:

$$\begin{aligned} \text{Var}[\dot{W}] &= \sum_r \left(\text{Var}[\dot{Q}_r] + 2 \sum_s \text{Cov}[\dot{Q}_r \dot{Q}_s] \right) \\ &= \omega_d^2 \text{Var}[\dot{N}]. \end{aligned} \quad (\text{B8})$$

where we have used Eqs. (B7).

Unfortunately the size and complexity of the matrix W_G in many cases makes impossible to obtain analytically the largest eigenvalue $\lambda(\{\chi_r\})$ by direct diagonalization of W_G , and other methods are required. In order to obtain the first and second cumulants analytically, we follow the method known as “Inverse Counting Statistics” originally introduced in Ref. [79] and used recently in Refs. [30, 33] for similar purposes. In the following we review this method for the case of a single field χ , which is enough for obtaining all the relevant quantities in our case, but the expressions can be naturally extended to multiple fields $\{\chi_r\}$ (see e.g. Appendix C in Ref. [33]).

In this method, the characteristic polynomial of W_G , namely, $\text{Pol}(\lambda) := -\det[W_G(\chi) - \lambda \mathbb{1}]$, is expanded in series in terms of the powers of its eigenvalues:

$$\text{Pol}(\lambda) = \sum_{n=0}^M a_n(\chi) \lambda^n(\chi) = 0, \quad (\text{B9})$$

where M is the range of the matrix W_G . Now we define the coefficients:

$$a'_n = i\partial_\chi a_n|_{\chi=0}, \quad (\text{B10})$$

$$a''_n = (i\partial_\chi)^2 a_n|_{\chi=0} = -\partial_\chi^2 a_n|_{\chi=0}, \quad (\text{B11})$$

and similarly denote $\lambda' = i\partial_\chi \lambda|_{\chi=0}$ and $\lambda'' = -\partial_\chi^2 \lambda|_{\chi=0}$. The first derivative of the entire characteristic polynomial is then given by:

$$\left[i\partial_\chi \sum_n a_n \lambda^n \right]_{\chi=0} = \sum_n [a'_n + (n+1)a_{n+1}\lambda'] \lambda^n(0), \quad (\text{B12})$$

and the second derivative reads:

$$\begin{aligned} \left[(-i\partial_\chi)^2 \sum_{n=0}^M a_n \lambda^n \right]_{\chi=0} &= \sum_{n=0}^M [a''_n + 2(n+1)a'_{n+1}\lambda' \\ &+ (n+1)a_{n+1}\lambda'' + (n+1)(n+2)a_{n+2}\lambda'^2] \lambda^n(0). \end{aligned} \quad (\text{B13})$$

Since $\text{Pol}(\lambda) = 0$, both equations above should be equal to zero. Therefore, if the system has a unique steady state, such that $\lambda(0) = 0$, as it is our case, then the zero order term in λ vanish, and we obtain from (B12):

$$a'_0 + a_1 \lambda' = 0, \quad (\text{B14})$$

so that the first cumulant (average current) is given by:

$$\mathcal{C}_1 = \lambda' = -\frac{a'_0}{a_1}, \quad (\text{B15})$$

and in the same way from (B13) we obtain the second cumulant (variance):

$$\mathcal{C}_2 = -\frac{1}{a_1} (a_0'' + a_1' \mathcal{C}_1 + a_2 \mathcal{C}_1^2). \quad (\text{B16})$$

Replacing the expression for the cumulant \mathcal{C}_1 in Eqs. B15 into the above Eq. (B16), we obtain the final expression for the variance of the probability current in the long-time limit:

$$\text{Var}[\dot{N}] = -\frac{1}{a_1} [a_0'' - a_1' \left(\frac{a_0'}{a_1} \right) + a_2 \left(\frac{a_0'}{a_1} \right)^2], \quad (\text{B17})$$

which is used to obtain all the variances for heat and work currents [Eqs. (B7) and (B8)]

Appendix C: Classical thermodynamic-equivalent models details

In this appendix we provide details on the procedure followed to obtain a classical thermodynamically equivalent model, in both cases of Hamiltonian-induced and noise-induced coherences. Moreover, we show that, even in the case of noise-induced coherence, it is sufficient that the classical analogue reproduces the steady-state populations in order to produce exactly the same steady state average currents.

We start by obtaining the equations of motion for the density operator elements from the master equation in Lindblad form (2), from which we can obtain the expression for a generic element of the density operator:

$$\dot{\rho}_{ij} = -i \langle i | [H(t), \rho] | j \rangle + \sum_r \sum_k \langle i | \mathcal{D}_k^{(r)}[\rho] | j \rangle. \quad (\text{C1})$$

After expanding the form of the dissipators $\mathcal{D}_k^{(r)}[\rho] = L_k^{(r)} \rho L_k^{(r)\dagger} - \frac{1}{2} \{ L_k^{(r)\dagger} L_k^{(r)}, \rho \}$, we obtain the following terms contributing to the above expression:

$$\begin{aligned} \langle i | [H(t), \rho] | j \rangle &= (\epsilon_j - \epsilon_i) \rho_{ij} + g(\delta_{iu} \rho_{vj} + \delta_{iv} \rho_{uj} \\ &\quad - \delta_{vj} \rho_{iu} - \delta_{uj} \rho_{iv}), \\ \langle i | L_k^{(r)} \rho L_k^{(r)\dagger} | j \rangle &= \sum_{n,m} \alpha_{ni}^k \alpha_{mj}^k \sqrt{\gamma_{ni} \gamma_{mj}} \rho_{nm}, \\ \langle i | L_k^{(r)\dagger} L_k^{(r)} \rho | j \rangle &= \sum_{n,m} \alpha_{im}^k \alpha_{nm}^k \sqrt{\gamma_{im} \gamma_{nm}} \rho_{nj}, \\ \langle i | \rho L_k^{(r)\dagger} L_k^{(r)} | j \rangle &= \sum_{n,m} \alpha_{nm}^k \alpha_{jm}^k \sqrt{\gamma_{nm} \gamma_{jm}} \rho_{in}, \end{aligned} \quad (\text{C2})$$

where we can again use the fact that the Lindblad operators produce jumps only between levels with a fixed energy gap $\Delta\epsilon_k = \pm\Delta\epsilon_r$, determined by the reservoirs and rewrite the α -terms as delta functions:

$$\begin{aligned} \alpha_{ni}^k \alpha_{mj}^k &= \delta(\Delta\epsilon_{in} - \Delta\epsilon_k) \delta(\Delta\epsilon_{jm} - \Delta\epsilon_k), \\ \alpha_{im}^k \alpha_{nm}^k &= \delta(\Delta\epsilon_{mi} - \Delta\epsilon_k) \delta(\Delta\epsilon_{ni}), \\ \alpha_{nm}^k \alpha_{jm}^k &= \delta(\Delta\epsilon_{mn} - \Delta\epsilon_k) \delta(\Delta\epsilon_{nj}). \end{aligned} \quad (\text{C3})$$

To specialize this result for the case of Hamiltonian-induced coherence we can use the fact that in (E4) first expression the only non-zero part is the second term, since the first will vanish, because we can always go to the interaction picture and consider only the interaction term of the total Hamiltonian (or in the non-energetic case both interacting levels have the same energy). On the other hand, the δ functions in (C3) can be simplified by taking into account the fact that in this case different transitions cannot have the same $\Delta\epsilon_k$ associated with them. Then (C3) becomes:

$$\begin{aligned} \alpha_{ni}^k \alpha_{mj}^k &= \delta(\Delta\epsilon_{in} - \Delta\epsilon_k) \delta_{ij} \delta_{nm}, \\ \alpha_{im}^k \alpha_{nm}^k &= \delta(\Delta\epsilon_{mi} - \Delta\epsilon_k) \delta_{ni}, \\ \alpha_{nm}^k \alpha_{jm}^k &= \delta(\Delta\epsilon_{mn} - \Delta\epsilon_k) \delta_{nj}. \end{aligned} \quad (\text{C4})$$

which results in the set of equations (23).

In the case of noise-induced coherence, we don't have an interaction Hamiltonian, so the first expression on (E4) doesn't need to be considered. The δ functions in (C3), on the other hand, have more terms, since there are now different transitions associated with the same $\Delta\epsilon_k$. Now (C3) reads:

$$\begin{aligned} \alpha_{ni}^k \alpha_{mj}^k &= \delta(\Delta\epsilon_{in} - \Delta\epsilon_k) (\delta_{ij} \delta_{nm} + \delta_{iu} \delta_{jv} \delta_{nm} + \delta_{iv} \delta_{ju} \delta_{nm} \\ &\quad + \delta_{nu} \delta_{mv} \delta_{ij} + \delta_{nv} \delta_{mu} \delta_{ij}), \\ \alpha_{im}^k \alpha_{nm}^k &= \delta(\Delta\epsilon_{mi} - \Delta\epsilon_k) (\delta_{ni} + \delta_{iv} \delta_{nu} + \delta_{iu} \delta_{nv}), \\ \alpha_{nm}^k \alpha_{jm}^k &= \delta(\Delta\epsilon_{mn} - \Delta\epsilon_k) (\delta_{nj} + \delta_{jv} \delta_{nu} + \delta_{ju} \delta_{nv}). \end{aligned} \quad (\text{C5})$$

In view of (C5) the equations of motion are:

$$\dot{\rho}_{nn} = \sum_i (\gamma_{in} \rho_{ii} - \gamma_{ni} \rho_{nn}) + 2\sqrt{\gamma_{un} \gamma_{vn}} \text{Re}(\rho_{uv}), \quad (\text{C6})$$

for the levels $n \neq \{u, v\}$, and:

$$\begin{aligned} \dot{\rho}_{nn} &= \sum_i [\gamma_{in} \rho_{ii} - (\gamma_{ni} \rho_{nn} + \sqrt{\gamma_{ui} \gamma_{vi}} \text{Re}(\rho_{uv}))], \\ \dot{\rho}_{uv} &= \sum_i [2\sqrt{\gamma_{ui} \gamma_{iv}} \rho_{ii} - \sqrt{\gamma_{ui} \gamma_{vi}} (\rho_{uu} + \rho_{vv}) \\ &\quad - (\gamma_{ui} + \gamma_{vi}) \rho_{uv}]. \end{aligned} \quad (\text{C7})$$

for $n = \{u, v\}$. They result in a steady-state coherence term given by (28). The introduction of (28) into (C7) leads to corrections for the rates and a new stochastic transition between levels u and v as shown in Eq. (29).

Finally, we show that all energy currents in the quantum machine and the classical equivalent are equal, also in the case of noise-induced coherence. Taking into account the fact that the transition in contact with the “work” reservoir is not involved in the noise inducing mechanism (involving only transitions from or to the degenerate levels), we observe that the classical equivalent can mimic the current $\langle \dot{Q}_w \rangle$ in the original machine if

it has the same populations in the steady state (since Eq. (22) depends only on the populations of the density matrix). Then, using Eq. (16), we also have that

$$\langle \dot{Q}_w \rangle = \langle \dot{Q}_w^{\text{cl}} \rangle \implies \langle \dot{N} \rangle = \langle \dot{N}^{\text{cl}} \rangle, \quad (\text{C8})$$

$\langle \dot{N}^{\text{cl}} \rangle$ being the corresponding probability current in the classical equivalent machine. The above relation stating the equivalence of the steady-state probability currents in quantum and classical engines implies, at the same time, that all the other energy currents in the original and classical equivalent machines are equal to their classical counterparts.

Appendix D: Expressions from Inverse Counting Statistics

In this appendix we provide the explicit form of the FCS matrix W_G and the relevant coefficients of the characteristic polynomial used to obtain analytical expressions for the currents variances using the Inverse Counting Statistics method, as introduced in App. B. For convenience we rewrite here the expressions of the probability flux in the long-time limit in terms of the rele-

vant coefficients for both the quantum machines and their classical-equivalent counterparts:

$$\begin{aligned} \text{Var}[\dot{N}] &= -\frac{1}{a_1} [a_0'' - a_1' \left(\frac{a_0'}{a_1} \right) + a_2 \left(\frac{a_0'}{a_1} \right)^2], \\ \text{Var}[\dot{N}^{\text{cl}}] &= -\frac{1}{a_1^{\text{cl}}} [a_0^{\text{cl}''} - a_1^{\text{cl}'} \left(\frac{a_0^{\text{cl}'}}{a_1^{\text{cl}}} \right) + a_2^{\text{cl}} \left(\frac{a_0^{\text{cl}'}}{a_1^{\text{cl}}} \right)^2], \end{aligned} \quad (\text{D1})$$

which are used to evaluate the variance of the different heat currents and power, as well as the fluctuations ratio \mathcal{R} as introduced in Eq. (31).

In the following subsections we first provide the expressions for the general cases of N -level multi-cycle machines discussed in Sec. V for Hamiltonian-induced coherence and noise-induced coherence, together with their corresponding classical equivalents. Then we also include the particular expressions for the three quantum thermal machines used as main illustrative examples in Sec. VI. We stress that while the explicit final expressions of $\text{Var}[\dot{N}]$ and $\text{Var}[\dot{N}^{\text{cl}}]$ as well as those of some of the coefficients are not included here for size reasons, all analytical expressions can be found in the supplemental GitHub repository [97].

1. Generic multi-cycle Hamiltonian-induced coherence machines

Following the coarse-graining procedure described in Sec. V we obtain the FCS matrix $W_G(\chi)$ in Eq. (B3) with a single counting field χ for quantum machines with Hamiltonian-induced coherence in one of their transitions. Recall that this matrix includes only the relation between the relevant coherences and the diagonal elements of the density matrix in the steady state, while those associated to coherences that become zero in the steady-state are not included. In the case of Hamiltonian-induced coherence this is the case of the coherent subspace (spanned by states $|u\rangle$ and $|v\rangle$), while coherences related to the monitoring state $|m\rangle$ or the coarse-grained state $|S\rangle$ (involving the rest of the system populations) are not included. Taking that into account, the matrix W_G associated to the vector $\vec{p}_G(t) = (\rho_{uu}, \rho_{vv}, \rho_{mm}, \rho_{ss}, \text{Im}[\rho_{uv}])$ has the form

$$W_G(\chi) = \begin{pmatrix} -\Gamma_{vs} & 0 & 0 & \Gamma_{sv} & -2g \\ 0 & -\gamma_{um} - \Gamma_{us} & e^{-i\chi}\gamma_{mu} & \Gamma_{su} & 2g \\ 0 & e^{i\chi}\gamma_{um} & -\Gamma_{ms} - \gamma_{mu} & \Gamma_{sm} & 0 \\ \Gamma_{vs} & \Gamma_{us} & \Gamma_{ms} & -\Gamma_{sm} - \Gamma_{su} - \Gamma_{sv} & 0 \\ g & -g & 0 & 0 & -\Gamma \end{pmatrix}, \quad (\text{D2})$$

where in the last row standing for the imaginary part of the coherence between states $|u\rangle$ and $|v\rangle$, we defined $\Gamma = (\Gamma_{vs} + \Gamma_{us} + \gamma_{um})/2$. The most relevant inverse counting coefficients associated with this matrix are (the rest can be found in the supplemental repository[97]):

$$\begin{aligned} a_0' &= \gamma_{mu}\Gamma_{sm} (\Gamma_{us} (2g^2 + \Gamma\Gamma_{vs}) + 2g^2\Gamma_{vs}) - \Gamma_{ms}\gamma_{um} (2g^2 (\Gamma_{su} + \Gamma_{sv}) + \Gamma\Gamma_{su}\Gamma_{vs}), \\ a_0'' &= \Gamma_{ms}\gamma_{um} (2g^2 (\Gamma_{su} + \Gamma_{sv}) + \Gamma\Gamma_{su}\Gamma_{vs}) + \gamma_{mu}\Gamma_{sm} (\Gamma_{us} (2g^2 + \Gamma\Gamma_{vs}) + 2g^2\Gamma_{vs}), \\ a_1' &= -[(\Gamma_{vs} + \Gamma)(\Gamma_{ms}\Gamma_{su}\gamma_{um} - \gamma_{mu}\Gamma_{sm}\Gamma_{us})]. \end{aligned} \quad (\text{D3})$$

For the classical equivalent of this model we no longer have the coherent contribution, but a new stochastic transition between the two levels involved in the coherent interaction with rates $\gamma_{vu}^{\text{cl}} = \gamma_{uv}^{\text{cl}}$ as given in Eq. (26). The matrix W_G^{cl}

in this case reads:

$$W_G^{\text{cl}}(\chi) = \begin{pmatrix} -\gamma_{\text{vu}}^{\text{cl}} - \Gamma_{\text{vs}} & \gamma_{\text{vu}}^{\text{cl}} & 0 & \Gamma_{\text{sv}} \\ \gamma_{\text{vu}}^{\text{cl}} & -\gamma_{\text{vu}}^{\text{cl}} - \gamma_{\text{um}} - \Gamma_{\text{us}} & e^{-i\chi} \gamma_{\text{mu}} & \Gamma_{\text{su}} \\ 0 & e^{i\chi} \gamma_{\text{um}} & -\Gamma_{\text{ms}} - \gamma_{\text{mu}} & \Gamma_{\text{sm}} \\ \Gamma_{\text{vs}} & \Gamma_{\text{us}} & \Gamma_{\text{ms}} & -\Gamma_{\text{sm}} - \Gamma_{\text{su}} - \Gamma_{\text{sv}} \end{pmatrix}, \quad (\text{D4})$$

which is associated to the reduced vector $\vec{p}_G^{\text{cl}}(t) = (\rho_{\text{uu}}, \rho_{\text{vv}}, \rho_{\text{mm}}, \rho_{\text{ss}})$. The associated relevant inverse counting coefficients (all coefficients can be found in [97]) are:

$$\begin{aligned} a_0^{\text{cl}\prime} &= \frac{\Gamma_{\text{ms}} \gamma_{\text{um}} (2g^2 (\Gamma_{\text{su}} + \Gamma_{\text{sv}}) + \Omega \Gamma_{\text{su}} \Gamma_{\text{vs}}) - \gamma_{\text{mu}} \Gamma_{\text{sm}} (\Gamma_{\text{us}} (2g^2 + \Omega \Gamma_{\text{vs}}) + 2g^2 \Gamma_{\text{vs}})}{\Gamma}, \\ a_0^{\text{cl}\prime\prime} &= -\frac{\Gamma_{\text{ms}} \gamma_{\text{um}} (2g^2 (\Gamma_{\text{su}} + \Gamma_{\text{sv}}) + \Omega \Gamma_{\text{su}} \Gamma_{\text{vs}}) + \gamma_{\text{mu}} \Gamma_{\text{sm}} (\Gamma_{\text{us}} (2g^2 + \Omega \Gamma_{\text{vs}}) + 2g^2 \Gamma_{\text{vs}})}{\Gamma}, \\ a_1^{\text{cl}\prime} &= \Gamma_{\text{ms}} \Gamma_{\text{su}} \gamma_{\text{um}} - \gamma_{\text{mu}} \Gamma_{\text{sm}} \Gamma_{\text{us}}. \end{aligned} \quad (\text{D5})$$

2. Three-level coherent amplifier

To obtain the form of W_G for this case, we write the system of equations for all elements of ρ_G given by (B1), using the Hamiltonian and Lindblad operators given in Sec. II A. We consider only the relevant elements of the matrix leading to non-zero values of the density operator π in the steady state. That is, we include terms connecting the level populations and the imaginary part of the coherence between states $|0\rangle$ and $|1\rangle$ (see Appendix C). On the other hand, both the real part of π_{12} and the real and imaginary part of the other coherences π_{13} and π_{23} become zero at the steady state and we don't need to describe their evolution. The matrix reads:

$$W_G = \begin{pmatrix} -\gamma_{02} & 0 & \gamma_{20} e^{-i\chi_h} & 2g \\ 0 & -\gamma_{12} & \gamma_{21} e^{-i\chi_c} & -2g \\ \gamma_{02} e^{i\chi_h} & \gamma_{12} e^{i\chi_c} & -(\gamma_{20} + \gamma_{21}) & 0 \\ g & -g & 0 & -\frac{1}{2}(\gamma_{02} + \gamma_{01}) \end{pmatrix},$$

associated to vector $\vec{p}_G(t) = (\rho_{00}, \rho_{11}, \rho_{22}, \text{Im}[\rho_{01}])$. The inverse counting coefficients are:

$$\begin{aligned} a_0' &= 2g^2 \gamma_c \gamma_h (\bar{n}_c - \bar{n}_h) \\ a_0'' &= -2g^2 \gamma_c \gamma_h (\bar{n}_c (2\bar{n}_h + 1) + \bar{n}_h) \\ a_1 &= \frac{1}{2} (\gamma_c (\bar{n}_c (\gamma_h^2 \bar{n}_h (3\bar{n}_h + 1) + 12g^2) + \gamma_h^2 \bar{n}_h^2 + 8g^2) + \gamma_c^2 \gamma_h \bar{n}_c (\bar{n}_c (3\bar{n}_h + 1) + \bar{n}_h) + 4g^2 \gamma_h (3\bar{n}_h + 2)) \\ a_2 &= \frac{1}{2} (\gamma_c \gamma_h (\bar{n}_c (10\bar{n}_h + 3) + 3\bar{n}_h) + \gamma_c^2 \bar{n}_c (2\bar{n}_c + 1) + \gamma_h^2 \bar{n}_h (2\bar{n}_h + 1) + 8g^2). \end{aligned} \quad (\text{D6})$$

and $a_1' = 0$.

In the case of the classical equivalent, we no longer consider the contribution of coherence to the dynamics, but introduce the classical stochastic transition rate between the interacting levels, leading to a matrix W_G^{cl} that reads:

$$W_G^{\text{cl}} = \begin{pmatrix} -(\gamma_{02} - \gamma_{10}^{\text{cl}}) & \gamma_{10}^{\text{cl}} & \gamma_{20} e^{-i\chi_h} \\ \gamma_{10}^{\text{cl}} & -(\gamma_{12} + \gamma_{10}^{\text{cl}}) & \gamma_{21} e^{-i\chi_c} \\ \gamma_{02} e^{i\chi_h} & \gamma_{12} e^{i\chi_c} & -(\gamma_{20} + \gamma_{21}) \end{pmatrix},$$

with the corresponding associated vector $\vec{p}_G^{\text{cl}}(t) = (\rho_{00}, \rho_{11}, \rho_{22})$. The associated inverse counting coefficients (all coefficients can be found in [97]) are:

$$\begin{aligned} a_0^{\text{cl}\prime} &= \frac{4g^2 \gamma_c \gamma_h (\bar{n}_h - \bar{n}_c)}{\gamma_c \bar{n}_c + \gamma_h \bar{n}_h} \\ a_0^{\text{cl}\prime\prime} &= \frac{4g^2 \gamma_c \gamma_h (\bar{n}_h - \bar{n}_c)}{\gamma_c \bar{n}_c + \gamma_h \bar{n}_h} \\ a_1^{\text{cl}} &= -\frac{8g^2 (\gamma_c + \gamma_h)}{\gamma_c \bar{n}_c + \gamma_h \bar{n}_h} - \gamma_c \gamma_h \bar{n}_c - \gamma_c \gamma_h (3\bar{n}_c + 1) \bar{n}_h - 12g^2 \\ a_2^{\text{cl}} &= -\frac{8g^2}{\gamma_c \bar{n}_c + \gamma_h \bar{n}_h} - \gamma_c (2\bar{n}_c + 1) - \gamma_h (2\bar{n}_h + 1). \end{aligned} \quad (\text{D7})$$

and again $a_1^{\text{cl}} = 0$.

3. Three-qubit autonomous refrigerator

Using the Hamiltonian and the Lindblad operators given in Sec. II B, we can derive in an analogous way the W_G matrices for the autonomous absorption refrigerator and its classical equivalent. Here again, we consider only relevant elements of the density matrix, which now consist of the populations of the 8 energy levels (in the three-qubit composed ladder) and a pure imaginary coherence between the states $|101\rangle$ and $|010\rangle$. The W_G matrix now have the form:

$$W_G = \begin{pmatrix} \Gamma_1 & \gamma_{10}^h e^{-i\chi_h} & \gamma_{10}^c e^{-i\chi_c} & 0 & 0 & 0 & 0 & \gamma_{10}^m e^{-i\chi_m} & 0 \\ \gamma_{01}^h e^{i\chi_h} & \Gamma_2 & 0 & \gamma_{10}^m e^{-i\chi_m} & 0 & 0 & \gamma_{10}^c e^{-i\chi_c} & 0 & 0 \\ \gamma_{01}^c e^{i\chi_c} & 0 & \Gamma_3 & 0 & \gamma_{10}^m e^{-i\chi_m} & 0 & \gamma_{10}^h e^{-i\chi_h} & 0 & 0 \\ 0 & \gamma_{01}^m e^{i\chi_m} & 0 & \Gamma_4 & 0 & \gamma_{10}^c e^{-i\chi_c} & 0 & \gamma_{01}^h e^{i\chi_h} & 0 \\ 0 & 0 & \gamma_{01}^m e^{i\chi_m} & 0 & \Gamma_5 & \gamma_{10}^h e^{-i\chi_h} & 0 & \gamma_{01}^c e^{i\chi_c} & 0 \\ 0 & 0 & 0 & \gamma_{01}^c e^{i\chi_c} & \gamma_{01}^h e^{i\chi_h} & \Gamma_6 & \gamma_{01}^m e^{i\chi_m} & 0 & 0 \\ 0 & \gamma_{01}^c e^{i\chi_c} & \gamma_{01}^h e^{i\chi_h} & 0 & 0 & \gamma_{10}^m e^{-i\chi_m} & \Gamma_7 & 0 & g \\ \gamma_{01}^m e^{i\chi_m} & 0 & 0 & \gamma_{10}^h e^{-i\chi_h} & \gamma_{10}^c e^{-i\chi_c} & 0 & 0 & \Gamma_8 & -g \\ 0 & 0 & 0 & 0 & 0 & 0 & -g & g & \Gamma_9 \end{pmatrix}$$

associated to vector $\vec{p}_G(t) = (\rho_{000}, \rho_{001}, \rho_{100}, \rho_{011}, \rho_{111}, \rho_{101}, \rho_{010}, \text{Im}[\rho_{010-101}])$. Some relevant inverse counting coefficients are in this case ((all coefficients can be found in [97])):

$$\begin{aligned} a'_0 &= 2g^2\gamma_c\gamma_h\gamma_m(\bar{n}_h(\bar{n}_c + \bar{n}_m + 1) - \bar{n}_c\bar{n}_m)(\gamma_c(2\bar{n}_c + 1) + \gamma_h(2\bar{n}_h + 1))(\gamma_c(2\bar{n}_c + 1) + \gamma_m(2\bar{n}_m + 1)) \\ &\quad (\gamma_h(2\bar{n}_h + 1) + \gamma_m(2\bar{n}_m + 1))(\gamma_c(2\bar{n}_c + 1) + \gamma_h(2\bar{n}_h + 1) + \gamma_m(2\bar{n}_m + 1)) \\ a''_0 &= 2g^2\gamma_c\gamma_h\gamma_m(\bar{n}_h(\bar{n}_c(2\bar{n}_m + 1) + \bar{n}_m + 1) + \bar{n}_c\bar{n}_m)(\gamma_c(2\bar{n}_c + 1) + \gamma_h(2\bar{n}_h + 1))(\gamma_c(2\bar{n}_c + 1) + \gamma_m(2\bar{n}_m + 1)) \\ &\quad (\gamma_h(2\bar{n}_h + 1) + \gamma_m(2\bar{n}_m + 1))(\gamma_c(2\bar{n}_c + 1) + \gamma_h(2\bar{n}_h + 1) + \gamma_m(2\bar{n}_m + 1)) \\ a'_1 &= 4g^2\gamma_c\gamma_h\gamma_m(\bar{n}_h(\bar{n}_c + \bar{n}_m + 1) - \bar{n}_c\bar{n}_m)(4\gamma_c^2(2\bar{n}_c + 1)^2(\gamma_h(2\bar{n}_h + 1) + \gamma_m(2\bar{n}_m + 1)) + \gamma_c(2\bar{n}_c + 1)(9\gamma_h\gamma_m(2\bar{n}_h + 1) \\ &\quad (2\bar{n}_m + 1) + 4\gamma_h^2(2\bar{n}_h + 1)^2 + 4\gamma_m^2(2\bar{n}_m + 1)^2) + \gamma_c^3(2\bar{n}_c + 1)^3 + (\gamma_h(2\bar{n}_h + 1) + \gamma_m(2\bar{n}_m + 1))(3\gamma_h\gamma_m(2\bar{n}_h + 1) \\ &\quad (2\bar{n}_m + 1) + \gamma_h^2(2\bar{n}_h + 1)^2 + \gamma_m^2(2\bar{n}_m + 1)^2)) \end{aligned} \quad (D8)$$

For the classical equivalent we instead loose the coherence contribution, while adding the extra rate γ^{cl} between degenerated levels:

$$W_G^{\text{cl}} = \begin{pmatrix} \Gamma_1 & \gamma_{10}^h e^{-i\chi_h} & \gamma_{10}^c e^{-i\chi_c} & 0 & 0 & 0 & 0 & \gamma_{10}^m e^{-i\chi_m} \\ \gamma_{01}^h e^{i\chi_h} & \Gamma_2 & 0 & \gamma_{10}^m e^{-i\chi_m} & 0 & 0 & \gamma_{10}^c e^{-i\chi_c} & 0 \\ \gamma_{01}^c e^{i\chi_c} & 0 & \Gamma_3 & 0 & \gamma_{10}^m e^{-i\chi_m} & 0 & \gamma_{10}^h e^{-i\chi_h} & 0 \\ 0 & \gamma_{01}^m e^{i\chi_m} & 0 & \Gamma_4 & 0 & \gamma_{10}^c e^{-i\chi_c} & 0 & \gamma_{01}^h e^{i\chi_h} \\ 0 & 0 & \gamma_{01}^m e^{i\chi_m} & 0 & \Gamma_5 & \gamma_{10}^h e^{-i\chi_h} & 0 & \gamma_{01}^c e^{i\chi_c} \\ 0 & 0 & 0 & \gamma_{01}^c e^{i\chi_c} & \gamma_{01}^h e^{i\chi_h} & \Gamma_6 & \gamma_{01}^m e^{i\chi_m} & 0 \\ 0 & \gamma_{01}^c e^{i\chi_c} & \gamma_{01}^h e^{i\chi_h} & 0 & 0 & \gamma_{10}^m e^{-i\chi_m} & \Gamma_7 - \gamma^{\text{cl}} & \gamma^{\text{cl}} \\ \gamma_{01}^m e^{i\chi_m} & 0 & 0 & \gamma_{10}^h e^{-i\chi_h} & \gamma_{10}^c e^{-i\chi_c} & 0 & \gamma^{\text{cl}} & \Gamma_8 - \gamma^{\text{cl}} \end{pmatrix}$$

for vector $\vec{p}_G^{\text{cl}}(t) = (\rho_{000}, \rho_{001}, \rho_{100}, \rho_{011}, \rho_{111}, \rho_{101}, \rho_{010})$. In the above equations, we defined $\Gamma_1 = -(\gamma_{01}^c + \gamma_{01}^m + \gamma_{01}^h)$, $\Gamma_2 = -(\gamma_{01}^c + \gamma_{01}^m + \gamma_{10}^h)$, $\Gamma_3 = -(\gamma_{10}^c + \gamma_{01}^m + \gamma_{01}^h)$, $\Gamma_4 = -(\gamma_{01}^c + \gamma_{10}^m + \gamma_{10}^h)$, $\Gamma_5 = -(\gamma_{10}^c + \gamma_{10}^m + \gamma_{01}^h)$, $\Gamma_6 = -(\gamma_{10}^c + \gamma_{10}^m + \gamma_{10}^h)$, $\Gamma_7 = -(\gamma_{10}^c + \gamma_{01}^m + \gamma_{10}^h)$, $\Gamma_8 = -(\gamma_{01}^c + \gamma_{10}^m + \gamma_{01}^h)$ and $\Gamma_9 = -\frac{1}{2}(\gamma_d + \gamma_{2d} + \gamma_{3d} + \gamma_u + \gamma_{2u} + \gamma_{3u})$. The corresponding

coefficients in the classical analog read:

$$\begin{aligned}
a_0^{\text{cl}'} &= -4g^2\gamma_c\gamma_h\gamma_m(\bar{n}_h(\bar{n}_c + \bar{n}_m + 1) - \bar{n}_c\bar{n}_m)(\gamma_c(2\bar{n}_c + 1) + \gamma_h(2\bar{n}_h + 1))(\gamma_c(2\bar{n}_c + 1) + \gamma_m(2\bar{n}_m + 1)) \\
&\quad (\gamma_h(2\bar{n}_h + 1) + \gamma_m(2\bar{n}_m + 1)) \\
a_0^{\text{cl}''} &= -4g^2\gamma_c\gamma_h\gamma_m(\bar{n}_h(\bar{n}_c(2\bar{n}_m + 1) + \bar{n}_m + 1) + \bar{n}_c\bar{n}_m)(\gamma_c(2\bar{n}_c + 1) + \gamma_h(2\bar{n}_h + 1))(\gamma_c(2\bar{n}_c + 1) + \gamma_m(2\bar{n}_m + 1)) \\
&\quad (\gamma_h(2\bar{n}_h + 1) + \gamma_m(2\bar{n}_m + 1)) \\
a_1^{\text{cl}'} &= -8g^2\gamma_c\gamma_h\gamma_m(\bar{n}_h(\bar{n}_c + \bar{n}_m + 1) - \bar{n}_c\bar{n}_m)(3\gamma_c(2\bar{n}_c + 1)(\gamma_h(2\bar{n}_h + 1) + \gamma_m(2\bar{n}_m + 1)) + \gamma_c^2(2\bar{n}_c + 1)^2 \\
&\quad + 3\gamma_h\gamma_m(2\bar{n}_h + 1)(2\bar{n}_m + 1) + \gamma_h^2(2\bar{n}_h + 1)^2 + \gamma_m^2(2\bar{n}_m + 1)^2),
\end{aligned} \tag{D9}$$

while the remanent coefficients are given in the repository [97].

4. Noise-induced-coherent machine

Finally, using the Hamiltonian and Lindblad operators from Sec. II C, we obtain the generic form of W_G for the noise-induced-coherence machine. In contrast with the previous cases, now we obtain non-zero real coherence in the steady state between states $|\alpha\rangle$ and $|\beta\rangle$ (see Appendix C). The relevant elements of the W_G matrix then connect the populations of the four levels and the real part of the coherence between states $|\alpha\rangle$ and $|\beta\rangle$:

$$W_G = \begin{pmatrix} -(\gamma_{0\alpha} + \gamma_{01}) & \gamma_{10} e^{-i\chi_w} & \gamma_{\alpha 0} e^{-i\chi_c} & 0 & 0 \\ \gamma_{01} e^{i\chi_w} & -(\gamma_{1\alpha} + \gamma_{1\beta} + \gamma_{10}) & \gamma_{\alpha 1} e^{-i\chi_h} & \gamma_{\beta 1} e^{-i\chi_h} & 2\sqrt{\gamma_{\alpha 1}\gamma_{\beta 1}} \\ \gamma_{0\alpha} e^{i\chi_c} & \gamma_{1\alpha} e^{i\chi_h} & -(\gamma_{\alpha 1} + \gamma_{\alpha 0}) & 0 & -\sqrt{\gamma_{\alpha 1}\gamma_{\beta 1}} \\ 0 & \gamma_{1\beta} e^{i\chi_h} & 0 & -\gamma_{\beta 1} & -\sqrt{\gamma_{\alpha 1}\gamma_{\beta 1}} \\ 0 & 2\sqrt{\gamma_{1\alpha}\gamma_{1\beta}} & -\sqrt{\gamma_{\alpha 1}\gamma_{\beta 1}} & -\sqrt{\gamma_{\alpha 1}\gamma_{\beta 1}} & \gamma_{\alpha 0} + \gamma_{\alpha 1} + \gamma_{\beta 1} \end{pmatrix},$$

with $\vec{p}_G(t) = (\rho_{00}, \rho_{11}, \rho_{\alpha\alpha}, \rho_{\beta\beta}, \text{Re}[\rho_{\alpha\beta}])$. Some relevant coefficients of the inverse counting method are (all coefficients can be found in [97]):

$$\begin{aligned}
a_0' &= \gamma_{\text{eg}}\bar{n}_c\bar{n}_h(\bar{n}_h - \bar{n}_c)(\gamma_c^\alpha)^2\gamma_h^\alpha\gamma_h^\beta \\
a_0'' &= \gamma_{\text{eg}}\bar{n}_c\bar{n}_h(\bar{n}_c(2\bar{n}_h + 1) + \bar{n}_h)(\gamma_c^\alpha)^2\gamma_h^\alpha\gamma_h^\beta \\
a_1 &= -\gamma_c^\alpha\gamma_h^\beta(\gamma_{\text{eg}}(\bar{n}_c(4\bar{n}_h + 1) + \bar{n}_h)(\bar{n}_c\gamma_c^\alpha + \bar{n}_h(\gamma_h^\alpha + \gamma_h^\beta)) + \bar{n}_c\bar{n}_h(\bar{n}_c(4\bar{n}_h + 3) + 3\bar{n}_h + 2)\gamma_c^\alpha\gamma_h^\alpha) \\
a_1' &= -\gamma_{\text{eg}}(\bar{n}_c - \bar{n}_h)\gamma_c^\alpha\gamma_h^\alpha(\bar{n}_c\gamma_c^\alpha + \bar{n}_h\gamma_h^\alpha).
\end{aligned} \tag{D10}$$

The matrix for the classical equivalent of the NIC machine does not contain the coherence anymore, but the modified rates $\{\gamma_{1\alpha}^{\text{cl}}, \gamma_{\alpha 1}^{\text{cl}}, \gamma_{1\beta}^{\text{cl}}, \gamma_{\beta 1}^{\text{cl}}, \gamma_{\alpha\beta}^{\text{cl}}\}$. It reads:

$$W_G^{\text{cl}} = \begin{pmatrix} -(\gamma_{0\alpha} + \gamma_{01}) & \gamma_{10} e^{-i\chi_w} & \gamma_{\alpha 0} e^{-i\chi_c} & 0 & \gamma_{\beta 1}^{\text{cl}} e^{-i\chi_h} \\ \gamma_{01} e^{i\chi_w} & -(\gamma_{1\alpha}^{\text{cl}} + \gamma_{1\beta}^{\text{cl}} + \gamma_{10}) & \gamma_{\alpha 1}^{\text{cl}} e^{-i\chi_h} & \gamma_{\beta 1}^{\text{cl}} e^{-i\chi_h} & \gamma_{\alpha\beta}^{\text{cl}} \\ \gamma_{0\alpha} e^{i\chi_c} & \gamma_{1\alpha}^{\text{cl}} e^{i\chi_h} & -(\gamma_{\alpha 1}^{\text{cl}} + \gamma_{\alpha 0} + \gamma_{\alpha\beta}^{\text{cl}}) & \gamma_{\alpha\beta}^{\text{cl}} & -(\gamma_{\beta 1}^{\text{cl}} + \gamma_{\alpha\beta}^{\text{cl}}) \\ 0 & \gamma_{1\beta}^{\text{cl}} e^{i\chi_h} & \gamma_{\alpha\beta}^{\text{cl}} & -(\gamma_{\beta 1}^{\text{cl}} + \gamma_{\alpha\beta}^{\text{cl}}) & \end{pmatrix},$$

with associated vector $\vec{p}_G^{\text{cl}}(t) = (\rho_{00}, \rho_{11}, \rho_{\alpha\alpha}, \rho_{\beta\beta})$. Some relevant coefficients in this case are:

$$\begin{aligned}
a_0^{\text{cl}'} &= \frac{\gamma_{\text{eg}}\bar{n}_c\bar{n}_h(\bar{n}_c - \bar{n}_h)(\gamma_c^\alpha)^2\gamma_h^\alpha\gamma_h^\beta}{\bar{n}_c\gamma_c^\alpha + \bar{n}_h(\gamma_h^\alpha + \gamma_h^\beta)} \\
a_0^{\text{cl}''} &= \frac{\gamma_{\text{eg}}\bar{n}_c\bar{n}_h(\bar{n}_c - \bar{n}_h)(\gamma_c^\alpha)^2\gamma_h^\alpha\gamma_h^\beta}{\bar{n}_c\gamma_c^\alpha + \bar{n}_h(\gamma_h^\alpha + \gamma_h^\beta)} \\
a_1^{\text{cl}} &= \gamma_c^\alpha\gamma_h^\beta\left(\gamma_{\text{eg}}(\bar{n}_c(4\bar{n}_h + 1) + \bar{n}_h) + \frac{\bar{n}_c\bar{n}_h(\bar{n}_c(4\bar{n}_h + 3) + 3\bar{n}_h + 2)\gamma_c^\alpha\gamma_h^\alpha}{\bar{n}_c\gamma_c^\alpha + \bar{n}_h(\gamma_h^\alpha + \gamma_h^\beta)}\right) \\
a_1^{\text{cl}'} &= \frac{\gamma_{\text{eg}}(\bar{n}_c - \bar{n}_h)\gamma_c^\alpha\gamma_h^\alpha(\bar{n}_c\gamma_c^\alpha + \bar{n}_h(\gamma_h^\alpha - \gamma_h^\beta))}{\bar{n}_c\gamma_c^\alpha + \bar{n}_h(\gamma_h^\alpha + \gamma_h^\beta)},
\end{aligned} \tag{D11}$$

the rest of them being given in the repository [97].

Appendix E: Proof of Theorem I

In this appendix we provide the proof of the Theorems 1 enunciated in Sec. V. The proof follows from the ana-

lytical evaluation of the sing of the ratio \mathcal{R} in Eq. (31), which can be reduced to the evaluation of the difference between the variances in quanum and classical-equivalent machines, $\text{Var}[\dot{N}^{\text{cl}}] - \text{Var}[\dot{N}]$. Using the explicit expressions for the variances from the Inverse Counting Statistics method (see App. B) provided in Eq. (D1), that difference can be written as:

$$\begin{aligned} \text{Var}[\dot{N}^{\text{cl}}] - \text{Var}[\dot{N}] &= \underbrace{\left(\frac{a_0''}{a_1} - \frac{a_0^{\text{cl}''}}{a_1^{\text{cl}}} \right)}_{(1)} \\ &+ 2\langle \dot{N} \rangle \underbrace{\left(\frac{a_1'}{a_1} - \frac{a_1^{\text{cl}'}}{a_1^{\text{cl}}} \right)}_{(2)} + 2\langle \dot{N} \rangle^2 \underbrace{\left(\frac{a_2}{a_1} - \frac{a_2^{\text{cl}}}{a_1^{\text{cl}}} \right)}_{(3)}, \end{aligned} \quad (\text{E1})$$

where we took advantage from the fact that, by construction of the classical equivalent, $\langle \dot{N} \rangle = \langle \dot{N}^{\text{cl}} \rangle$. In the following we evaluate the three under-brace terms in Eq. (E1) for the inverse counting coefficients obtained for Hamiltonian-induced coherence [Eqs. (D3) and (D5)]. For the first term (1) we obtain always a vanishing contribution:

$$\left(\frac{a_0''}{a_1} - \frac{a_0^{\text{cl}''}}{a_1^{\text{cl}}} \right) = 0, \quad (\text{E2})$$

and therefore it does not contribute to Eq. (E1). For the third term (3) in Eq. (E1) we have instead:

$$\left(\frac{a_2}{a_1} - \frac{a_2^{\text{cl}}}{a_1^{\text{cl}}} \right) = \frac{1}{Z} \sum_{i \neq i'} \sum_{j \neq j'} \sum_{k \neq k'} \Gamma_{ii'} \Gamma_{jj'} \Gamma_{kk'} \geq 0 \quad (\text{E3})$$

which is always positive since the rates are positive and $Z > 0$ is a positive (normalization) factor. Moreover since this term is multiplied by $\langle \dot{N} \rangle^2$ in Eq. (E1), it always leads to a positive contribution to $\text{Var}[\dot{N}^{\text{cl}}] - \text{Var}[\dot{N}]$.

On the other hand for the term (2) in Eq. (E1) we have:

$$\begin{aligned} \left(\frac{a_1'}{a_1} - \frac{a_1^{\text{cl}'}}{a_1^{\text{cl}}} \right) &= \frac{1}{Z} (\Gamma_{vs} (\Gamma_{ms} \Gamma_{su} \gamma_{um} - \gamma_{mu} \Gamma_{sm} \Gamma_{us}) \\ &+ \gamma_{vm} (\gamma_{um} \Gamma_{ms} \Gamma_{su} - \gamma_{mu} \Gamma_{us} \Gamma_{sm}) \\ &+ (\gamma_{mu} \Gamma_{us} \Gamma_{sv} \gamma_{vm} - \gamma_{um} \gamma_{mv} \Gamma_{vs} \Gamma_{su})) \end{aligned} \quad (\text{E4})$$

where differences between the rates associated to certain cycles in opposite directions appear. Notably, however, none of such cycles involve the coherent transition between levels $|u\rangle$ and $|v\rangle$. Now we show that the contribution in Eq. (E4) is zero in the cases of unicyclic and multicycle (multipartite) quantum thermal machines. First, in the case of unicyclic machines we will (trivially) have $\Gamma_{us} = \Gamma_{su} = 0$ and $\Gamma_{vm} = \Gamma_{mv} = 0$, which makes all the different terms in Eq. (E4) equal to zero. Second, we consider a multicycle structure in the thermal machine where all cycles have the same number of contributions from the different baths. This is the case e.g. of multipartite systems under local dissipation. In that case we

have that to close cycles that do not include the coherent transition between the levels $|u\rangle$ and $|v\rangle$, we will have the same number of quanta in and out from each given bath during the cycle (see e.g. Fig. 2b for an illustration) and therefore there will be no net probability flux in one or the other direction. This property implies that three three parenthesis in Eq. (E4) cancel.

As a consequence of the above analysis, we have that the fluctuation ratio \mathcal{R} is given by the following expression:

$$\mathcal{R} = \frac{\langle \dot{N} \rangle^2}{Z} \sum_{i \neq i'} \sum_{j \neq j'} \sum_{k \neq k'} \Gamma_{ii'} \Gamma_{jj'} \Gamma_{kk'} \geq 0 \quad (\text{E5})$$

which is always greater than zero in out-of-equilibrium scenarios. Since \mathcal{R} is strictly greater than zero just in the case of $\langle \dot{N} \rangle \neq 0$ which corresponds with the out-of-equilibrium scenario.

Appendix F: Details on the NIC machine

In this appendix we discuss in more detail the change of variables introduced in Sec. V C to decouple one of the two collective transitions of the NIC coherent machine, together with extra comments regarding the symmetric limit in which all the spontaneous emission rates are equal.

Once we have introduced the change of variable (37) we can rewrite the set of new Lindblad operators as

$$\begin{aligned} L_{\downarrow}^{(c)} &= \sqrt{\gamma_{\alpha 0}} |0\rangle \langle \alpha|, \quad L_{\uparrow}^{(c)} = \sqrt{\gamma_{0\alpha}} |\alpha\rangle \langle 0|, \\ L_{\downarrow}^{(h)} &= \sqrt{\gamma_{\alpha 1}} |1\rangle \langle \alpha| + \sqrt{\gamma_{\beta 1}} |1\rangle \langle \beta|, \\ L_{\uparrow}^{(h)} &= \sqrt{\gamma_{1\alpha}} |\alpha\rangle \langle 1| + \sqrt{\gamma_{1\beta}} |\beta\rangle \langle 1|, \end{aligned} \quad (\text{F1})$$

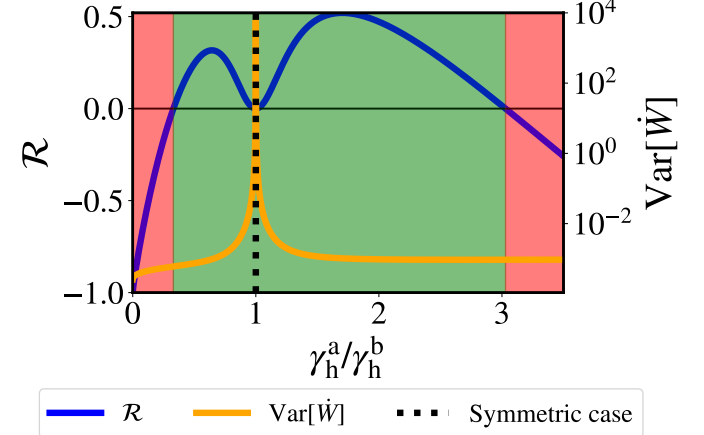


FIG. 10. Fluctuations ratio \mathcal{R} (blue solid line) and variance in the quantum system (orange dotted line) as functions of the ratio of the original spontaneous emission rates (prior to the change of variables). The system parameters are: $\beta_w \rightarrow 0$, $\beta_c = 1$, $\beta_h/\beta_c = 0.9$, $\epsilon_2 = 5$, $\epsilon_1 = 3$, and $\gamma_c^{(a/b)} = 10^{-3}$ (energies are given in units of $k_B T_c = 1$).

where the different transitions are mediated by the same thermal baths as before, i.e. $\gamma_{00} = (\bar{n}_c + 1)\gamma_c^\alpha$, $\gamma_{0\alpha} = \bar{n}_c\gamma_c^\alpha$, $\gamma_{\alpha 1} = (\bar{n}_h + 1)\gamma_h^\alpha$, $\gamma_{1\alpha} = \bar{n}_h\gamma_h^\alpha$, $\gamma_{\beta 1} = (\bar{n}_h + 1)\gamma_h^\beta$, $\gamma_{1\beta} = \bar{n}_h\gamma_h^\beta$; and we can identify the new spontaneous emission rates:

$$\begin{aligned}\gamma_c^\alpha &= \gamma_c^a + \gamma_c^b, \\ \gamma_h^\alpha &= (\sqrt{\gamma_c^a \gamma_h^a} + \sqrt{\gamma_c^b \gamma_h^b})^2 / (\gamma_c^a + \gamma_c^b), \\ \gamma_h^\beta &= (\sqrt{\gamma_c^a \gamma_h^b} - \sqrt{\gamma_c^b \gamma_h^a})^2 / (\gamma_c^a + \gamma_c^b).\end{aligned}\quad (\text{F2})$$

For symmetric rates, we recover the situation where $|\beta\rangle$ is completely decoupled from the states $|0\rangle$ and $|1\rangle$ ($\gamma_h^\beta = 0$), leading to a classical three-level system with local jumps induced by thermal baths at same temperatures than the original NIC machine, plus an extra uncoupled level (dark state). Considering Eqs. (38), (39) and (40), it becomes evident that in this limit, the quantum system and its classical analog become indistinguishable once the

probability of the independent (dark) level is set to zero. On the other hand, if we approach this symmetric case asymptotically, the first inequality in Eq. (41) indicates that, in principle, the quantum system is more precise than the classical equivalent. However, it is important to note that in this limit, fluctuations in the system currents will diverge due to a first-order phase transition, as shown in Ref. [69]. That leads to $\mathcal{R} = 0$ as can be appreciated in Fig. 10 for $\gamma_h^a = \gamma_h^b$, where $\text{Var}[\dot{W}]$ diverges (vertical dotted line). The green and red areas in Fig. 10 represent respectively the regions of parameters where quantum advantage or disadvantages are obtained. This finding aligns with the observation that, in the symmetric case, the change of variables completely decouples coherences from populations. As mentioned before, in that case one can always redefine the relevant thermal machine under consideration by excluding the independent (dark) level. In that case, the remaining (connected) thermal machine will be exactly equal as their classical counterpart.

[1] F. Binder, L. A. Correa, C. Gogolin, J. Anders, and G. Adesso, eds., *Thermodynamics in the Quantum Regime* (Springer, Cham, 2018).

[2] G. T. Landi and M. Paternostro, Irreversible entropy production: From classical to quantum, *Rev. Mod. Phys.* **93**, 035008 (2021).

[3] H. E. D. Scovil and E. O. Schulz-DuBois, Three-level masers as heat engines, *Phys. Rev. Lett.* **2**, 262 (1959).

[4] E. Geva and R. Kosloff, Three-level quantum amplifier as a heat engine: A study in finite-time thermodynamics, *Phys. Rev. E* **49**, 3903 (1994).

[5] E. Boukobza and D. J. Tannor, Three-level systems as amplifiers and attenuators: A thermodynamic analysis, *Phys. Rev. Lett.* **98**, 240601 (2007).

[6] N. Linden, S. Popescu, and P. Skrzypczyk, How small can thermal machines be? the smallest possible refrigerator, *Phys. Rev. Lett.* **105**, 130401 (2010).

[7] A. Levy and R. Kosloff, Quantum absorption refrigerator, *Phys. Rev. Lett.* **108**, 070604 (2012).

[8] N. Brunner, N. Linden, S. Popescu, and P. Skrzypczyk, Virtual qubits, virtual temperatures, and the foundations of thermodynamics, *Phys. Rev. E* **85**, 051117 (2012).

[9] R. Uzdin, A. Levy, and R. Kosloff, Equivalence of quantum heat machines, and quantum-thermodynamic signatures, *Phys. Rev. X* **5**, 031044 (2015).

[10] J. Roßnagel, S. T. Dawkins, K. N. Tolazzi, O. Abah, E. Lutz, F. Schmidt-Kaler, and K. Singer, A single-atom heat engine, *Science* **352**, 325 (2016).

[11] G. Maslennikov, S. Ding, R. Hablitzel, J. Gan, A. Roulet, S. Nimmrichter, J. Dai, V. Scarani, and D. Matsukevich, Quantum absorption refrigerator with trapped ions, *Nat. Commun.* **10**, 202 (2019).

[12] J. Klatzow, J. N. Becker, P. M. Ledingham, C. Weinzel, K. T. Kaczmarek, D. J. Saunders, J. Nunn, I. A. Walmsley, R. Uzdin, and E. Poem, Experimental demonstration of quantum effects in the operation of microscopic heat engines, *Phys. Rev. Lett.* **122**, 110601 (2019).

[13] N. M. Myers, O. Abah, and S. Deffner, Quantum thermodynamic devices: From theoretical proposals to experimental reality, *AVS Quantum Science* **4**, 027101 (2022), https://pubs.aip.org/avs/aqs/article-pdf/doi/10.1116/5.0083192/16494008/027101_1_online.pdf.

[14] M. O. Scully, M. S. Zubairy, G. S. Agarwal, and H. Walther, Extracting work from a single heat bath via vanishing quantum coherence, *Science* **299**, 862 (2003), <https://www.science.org/doi/pdf/10.1126/science.1078955>.

[15] R. Kosloff and A. Levy, Quantum heat engines and refrigerators: Continuous devices, *Annu. Rev. Phys. Chem.* **65**, 365 (2014).

[16] M. O. Scully, K. R. Chapin, K. E. Dorfman, M. B. Kim, and A. Svidzinsky, Quantum heat engine power can be increased by noise-induced coherence, *Proceedings of the National Academy of Sciences* **108**, 15097 (2011), <https://www.pnas.org/doi/pdf/10.1073/pnas.1110234108>.

[17] D. Gelbwaser-Klimovsky, W. Niedenzu, P. Brumer, and G. Kurizki, Power enhancement of heat engines via correlated thermalization in a three-level working fluid, *Sci. Rep.* **5**, 14413 (2015).

[18] J. Um, K. E. Dorfman, and H. Park, Coherence-enhanced quantum-dot heat engine, *Phys. Rev. Res.* **4**, L032034 (2022).

[19] K. E. Dorfman, D. V. Voronine, S. Mukamel, and M. O. Scully, Photosynthetic reaction center as a quantum heat engine, *Proceedings of the National Academy of Sciences* **110**, 2746 (2013), <https://www.pnas.org/doi/pdf/10.1073/pnas.1212666110>.

[20] N. Brunner, M. Huber, N. Linden, S. Popescu, R. Silva, and P. Skrzypczyk, Entanglement enhances cooling in microscopic quantum refrigerators, *Phys. Rev. E* **89**, 032115 (2014).

[21] M. T. Mitchison, M. P. Woods, J. Prior, and M. Huber, Coherence-assisted single-shot cooling by quantum absorption refrigerators, *New Journal of Physics* **17**, 115013 (2015).

[22] G. Manzano, G.-L. Giorgi, R. Fazio, and R. Zambrini, Boosting the performance of small autonomous refriger-

ators via common environmental effects, *New Journal of Physics* **21**, 123026 (2019).

[23] J. O. González, J. P. Palao, D. Alonso, and L. A. Correa, Classical emulation of quantum-coherent thermal machines, *Phys. Rev. E* **99**, 062102 (2019).

[24] A. C. Barato and U. Seifert, Thermodynamic uncertainty relation for biomolecular processes, *Phys. Rev. Lett.* **114**, 158101 (2015).

[25] T. R. Gingrich, J. M. Horowitz, N. Perunov, and J. L. England, Dissipation bounds all steady-state fluctuations, *Phys. Rev. Lett.* **116**, 120601 (2016).

[26] J. M. Horowitz and T. R. Gingrich, Thermodynamic uncertainty relations constrain non-equilibrium fluctuations, *Nat. Phys.* **16**, 15 (2020).

[27] P. Pietzonka and U. Seifert, Universal trade-off between power, efficiency, and constancy in steady-state heat engines, *Phys. Rev. Lett.* **120**, 190602 (2018).

[28] K. Ptaszyński, Coherence-enhanced constancy of a quantum thermoelectric generator, *Phys. Rev. B* **98**, 085425 (2018).

[29] J. Liu and D. Segal, Thermodynamic uncertainty relation in quantum thermoelectric junctions, *Phys. Rev. E* **99**, 062141 (2019).

[30] A. A. S. Kalaei, A. Wacker, and P. P. Potts, Violating the thermodynamic uncertainty relation in the three-level maser, *Phys. Rev. E* **104**, L012103 (2021).

[31] A. Rignon-Bret, G. Guarnieri, J. Goold, and M. T. Mitchison, Thermodynamics of precision in quantum nanomachines, *Phys. Rev. E* **103**, 012133 (2021).

[32] L. d. S. Souza, G. Manzano, R. Fazio, and F. Iemini, Collective effects on the performance and stability of quantum heat engines, *Phys. Rev. E* **106**, 014143 (2022).

[33] G. Manzano and R. López, Quantum-enhanced performance in superconducting andreev reflection engines, *Phys. Rev. Res.* **5**, 043041 (2023).

[34] L. F. Seoane and R. V. Solé, A multiobjective optimization approach to statistical mechanics, *arXiv: Statistical Mechanics* (2013).

[35] L. Dinis, J. Unterberger, and D. Lacoste, Phase transitions in optimal betting strategies, *Europhysics Letters* **131**, 60005 (2020).

[36] L. Dinis, J. Unterberger, and D. Lacoste, Pareto-optimal trade-off for phenotypic switching of populations in a stochastic environment, *Journal of Statistical Mechanics: Theory and Experiment* **2022**, 053503 (2022).

[37] A. P. Solon and J. M. Horowitz, Phase transition in protocols minimizing work fluctuations, *Phys. Rev. Lett.* **120**, 180605 (2018).

[38] P. A. Erdman, A. Rolandi, P. Abiuso, M. Perarnau-Llobet, and F. Noé, Pareto-optimal cycles for power, efficiency and fluctuations of quantum heat engines using reinforcement learning, *Phys. Rev. Res.* **5**, L022017 (2023).

[39] H. J. D. Miller and M. Mehboodi, Geometry of work fluctuations versus efficiency in microscopic thermal machines, *Phys. Rev. Lett.* **125**, 260602 (2020).

[40] H.-P. Breuer and F. Petruccione, *The Theory of Open Quantum Systems* (OXFORD University Press, 2002).

[41] Ángel Rivas and S. F. Huelga, *Open Quantum Systems. An introduction* (Springer, 2012).

[42] G. D. Chiara, G. Landi, A. Hewgill, B. Reid, A. Ferraro, A. J. Roncaglia, and M. Antezza, Reconciliation of quantum local master equations with thermodynamics, *New Journal of Physics* **20**, 113024 (2018).

[43] P. P. Hofer, M. Perarnau-Llobet, L. D. M. Miranda, G. Haack, R. Silva, J. B. Brask, and N. Brunner, Markovian master equations for quantum thermal machines: local versus global approach, *New Journal of Physics* **19**, 123037 (2017).

[44] A. S. Trushechkin and I. V. Volovich, Perturbative treatment of inter-site couplings in the local description of open quantum networks, *Europhysics Letters* **113**, 30005 (2016).

[45] J. E. Geusic, E. O. Schulz-DuBios, and H. E. D. Scovil, Quantum equivalent of the carnot cycle, *Phys. Rev.* **156**, 343 (1967).

[46] J. P. Palao, R. Kosloff, and J. M. Gordon, Quantum thermodynamic cooling cycle, *Phys. Rev. E* **64**, 056130 (2001).

[47] S.-W. Li, M. B. Kim, G. S. Agarwal, and M. O. Scully, Quantum statistics of a single-atom scovil-schulz-dubois heat engine, *Phys. Rev. A* **96**, 063806 (2017).

[48] K. E. Dorfman, D. Xu, and J. Cao, Efficiency at maximum power of a laser quantum heat engine enhanced by noise-induced coherence., *Phys. Rev. E* **97** (2018).

[49] S. Varinder, Optimal operation of a three-level quantum heat engine and universal nature of efficiency., *Phys. Rev. Research* **2** (2020).

[50] P. Skrzypczyk, N. Brunner, N. Linden, and S. Popescu, The smallest refrigerators can reach maximal efficiency, *Journal of Physics A: Mathematical and Theoretical* **44**, 492002 (2011).

[51] R. Silva, G. Manzano, P. Skrzypczyk, and N. Brunner, Performance of autonomous quantum thermal machines: Hilbert space dimension as a thermodynamical resource, *Phys. Rev. E* **94**, 032120 (2016).

[52] L. A. Correa, J. P. Palao, G. Adesso, and D. Alonso, Performance bound for quantum absorption refrigerators, *Phys. Rev. E* **87**, 042131 (2013).

[53] L. A. Correa, J. P. Palao, G. Adesso, and D. Alonso, Optimal performance of endoreversible quantum refrigerators., *Phys. Rev. E* **90** (2014).

[54] L. A. Correa, J. P. Palao, D. Alonso, and G. Adesso, Quantum-enhanced absorption refrigerators, *Scientific Reports* **21** (2014).

[55] S. Seah, S. Nimmrichter, and V. Scarani, Refrigeration beyond weak internal coupling, *Phys. Rev. E* **98**, 012131 (2018).

[56] D. Venturelli, R. Fazio, and V. Giovannetti, Minimal self-contained quantum refrigeration machine based on four quantum dots, *Phys. Rev. Lett.* **110**, 256801 (2013).

[57] M. T. Mitchison, M. Huber, J. Prior, M. P. Woods, and M. B. Plenio, Realising a quantum absorption refrigerator with an atom-cavity system, *Quantum Science and Technology* **1**, 015001 (2016).

[58] P. P. Hofer, M. Perarnau-Llobet, J. B. Brask, R. Silva, M. Huber, and N. Brunner, Autonomous quantum refrigerator in a circuit qed architecture based on a josephson junction, *Phys. Rev. B* **94**, 235420 (2016).

[59] M. O. Scully, Quantum photocell: Using quantum coherence to reduce radiative recombination and increase efficiency, *Phys. Rev. Lett.* **104**, 207701 (2010).

[60] V. V. Kozlov, Y. Rostovtsev, and M. O. Scully, Inducing quantum coherence via decays and incoherent pumping with application to population trapping, lasing without inversion, and quenching of spontaneous emission, *Phys. Rev. A* **74**, 063829 (2006).

[61] T. V. Tscherbul and P. Brumer, Long-lived quasistation-

ary coherences in a v-type system driven by incoherent light., *Phys. Rev. Lett.* **113** (2014).

[62] U. Harbola, S. Rahav, and S. Mukamel, Quantum heat engines: A thermodynamic analysis of power and efficiency, *Europhysics Letters* **99**, 50005 (2012).

[63] H. P. Goswami and U. Harbola, Thermodynamics of quantum heat engines, *Phys. Rev. A* **88**, 013842 (2013).

[64] N. Killoran, S. F. Huelga, and M. B. Plenio, Enhancing light-harvesting power with coherent vibrational interactions: A quantum heat engine picture., *J. Chem. Phys.* **143** (2015).

[65] C.-P. S. Shan-He Su, S.-W. Li, and J.-C. Chen, Photoelectric converters with quantum coherence., *Phys. Rev. E* **93** (2016).

[66] V. Holubec and T. Novotný, Effects of noise-induced coherence on the performance of quantum absorption refrigerators., *J. Low Temp. Phys.* **192** (2018).

[67] C. L. Latune, I. Sinayskiy, and F. Petruccione, Apparent temperature: demystifying the relation between quantum coherence, correlations, and heat flows, *Quantum Science and Technology* **4**, 025005 (2019).

[68] J. Liu and D. Segal, Coherences and the thermodynamic uncertainty relation: Insights from quantum absorption refrigerators, *Phys. Rev. E* **103**, 032138 (2021).

[69] V. Holubec and T. Novotný, Effects of noise-induced coherence on the fluctuations of current in quantum absorption refrigerators., *J. Chem. Phys.* **151** (2019).

[70] R. Alicki, The quantum open system as a model of the heat engine, *Journal of Physics A: Mathematical and General* **12**, L103 (1979).

[71] G. Manzano, J. M. Horowitz, and J. M. R. Parrondo, Quantum fluctuation theorems for arbitrary environments: Adiabatic and nonadiabatic entropy production, *Phys. Rev. X* **8**, 031037 (2018).

[72] G. Manzano and R. Zambrini, Quantum thermodynamics under continuous monitoring: A general framework, *AVS Quantum Science* **4**, 025302 (2022).

[73] A. Hewgill, G. De Chiara, and A. Imparato, Quantum thermodynamically consistent local master equations, *Phys. Rev. Res.* **3**, 013165 (2021).

[74] P. Strasberg, G. Schaller, T. Brandes, and M. Esposito, Quantum and information thermodynamics: A unifying framework based on repeated interactions, *Phys. Rev. X* **7**, 021003 (2017).

[75] G. Manzano, R. Sánchez, R. Silva, G. Haack, J. B. Brask, N. Brunner, and P. P. Potts, Hybrid thermal machines: Generalized thermodynamic resources for multitasking, *Phys. Rev. Res.* **2**, 043302 (2020).

[76] R. López, J. S. Lim, and K. W. Kim, Optimal superconducting hybrid machine, *Phys. Rev. Res.* **5**, 013038 (2023).

[77] K. Hammam, G. Manzano, and G. De Chiara, Quantum coherence enables hybrid multitask and multisource regimes in autonomous thermal machines, *Phys. Rev. Res.* **6**, 013310 (2024).

[78] M. Esposito, U. Harbola, and S. Mukamel, Nonequilibrium fluctuations, fluctuation theorems, and counting statistics in quantum systems, *Rev. Mod. Phys.* **81**, 1665 (2009).

[79] M. Bruderer, L. D. Contreras-Pulido, M. Thaller, L. Sironi, D. Obreschkow, and M. B. Plenio, Inverse counting statistics for stochastic and open quantum systems: the characteristic polynomial approach, *New Journal of Physics* **16**, 033030 (2014).

[80] M. Esposito, Stochastic thermodynamics under coarse graining, *Phys. Rev. E* **85**, 041125 (2012).

[81] We notice that it is not convenient to apply the FCS formalism to the transitions inside S since, once defined the mesostate, it is not possible anymore to associate an specific energy exchange to any transition from or to S .

[82] M. Campisi, J. Pekola, and R. Fazio, Nonequilibrium fluctuations in quantum heat engines: theory, example, and possible solid state experiments, *New Journal of Physics* **17**, 035012 (2015).

[83] M. T. Naseem, A. Misra, and Özgür E Müstecaplıoğlu, Two-body quantum absorption refrigerators with optomechanical-like interactions, *Quantum Science and Technology* **5**, 035006 (2020).

[84] H. Thierschmann, R. Sánchez, B. Sothmann, F. Arnold, C. Heyn, W. Hansen, H. Buhmann, and L. W. Molenkamp, Three-terminal energy harvester with coupled quantum dots, *Nature Nanotechnology* **10**, 854 (2015).

[85] Y. Zou, Y. Jiang, Y. Mei, X. Guo, and S. Du, Quantum heat engine using electromagnetically induced transparency, *Phys. Rev. Lett.* **119**, 050602 (2017).

[86] J.-W. Zhang, J.-Q. Zhang, G.-Y. Ding, J.-C. Li, J.-T. Bu, B. Wang, L.-L. Yan, S.-L. Su, L. Chen, F. Nori, A. Özdemir, F. Zhou, H. Jing, and M. Feng, Dynamical control of quantum heat engines using exceptional points, *Nature communications* **13**, 6225 (2022).

[87] P. P. Hofer, J.-R. Souquet, and A. A. Clerk, Quantum heat engine based on photon-assisted cooper pair tunneling, *Phys. Rev. B* **93**, 041418 (2016).

[88] R. Sánchez, P. Burset, and A. L. Yeyati, Cooling by cooper pair splitting, *Phys. Rev. B* **98**, 241414 (2018).

[89] F. Carollo, K. Brandner, and I. Lesanovsky, Nonequilibrium many-body quantum engine driven by time-translation symmetry breaking, *Phys. Rev. Lett.* **125**, 240602 (2020).

[90] J. B. Brask, G. Haack, N. Brunner, and M. Huber, Autonomous quantum thermal machine for generating steady-state entanglement, *New Journal of Physics* **17**, 113029 (2015).

[91] P. Erker, M. T. Mitchison, R. Silva, M. P. Woods, N. Brunner, and M. Huber, Autonomous quantum clocks: Does thermodynamics limit our ability to measure time?, *Phys. Rev. X* **7**, 031022 (2017).

[92] S. Khandelwal, N. Brunner, and G. Haack, Signatures of liouvillian exceptional points in a quantum thermal machine, *PRX Quantum* **2**, 040346 (2021).

[93] E. Goodarzi, M. Ziae, and E. Z. Hosseinpour, *Introduction to Optimization Analysis in Hydrosystem Engineering* (Springer International Publishing, 2014).

[94] G. T. Landi, M. J. Kewming, M. T. Mitchison, and P. P. Potts, Current fluctuations in open quantum systems: Bridging the gap between quantum continuous measurements and full counting statistics, *PRX Quantum* **5**, 020201 (2024).

[95] S. Pal, S. Saryal, D. Segal, T. S. Mahesh, and B. K. Agarwalla, Experimental study of the thermodynamic uncertainty relation, *Phys. Rev. Res.* **2**, 022044 (2020).

[96] G. Schaller, *Open Quantum Systems Far from Equilibrium* (Springer International Publishing, 2014).

[97] <https://github.com/ja-almanza-marrero/supplemental-material-continious-thermal-machines->